

# Cold atom-dimer reaction rates with $^4\text{He}$ , $^6,^7\text{Li}$ and $^{23}\text{Na}$

M. A. Shalchi<sup>1</sup>, M. T. Yamashita<sup>1</sup>, T. Frederico<sup>2</sup> and Lauro Tomio<sup>1</sup>

<sup>1</sup> *Instituto de Física Teórica, Universidade Estadual Paulista, 01405-900 São Paulo, Brasil.*

<sup>2</sup> *Instituto Tecnológico de Aeronáutica, DCTA, 12228-900 São José dos Campos, Brasil.*

(Dated: May 25, 2022)

Atom-dimer exchange and dissociation reaction rates are predicted for different combinations of two  $^4\text{He}$  atoms and one of the alkaline species among  $^6\text{Li}$ ,  $^7\text{Li}$  and  $^{23}\text{Na}$ , by using three-body scattering formalism with short-range two-body interactions. Our study was concerned with low-energy reaction rates in which the  $s$ -,  $p$ - and  $d$ - wave contributions are the relevant ones. The  $^4\text{He}$  is chosen as one of the atoms in the binary mixture, in view of previous available investigations and laboratory accessibilities. Focusing on possible experimental cold-atom realizations with two-atomic mixtures, in which information on atom-dimer reaction rates can be extracted, we predict the occurrence of a dip in the elastic reaction rate for colliding energies smaller than 20 mK, when the dimer is the  $^4\text{He}^{23}\text{Na}$  molecule. We are also anticipating a zero in the elastic  $p$ -wave contribution for the  $^4\text{He} + ^4\text{He}^7\text{Li}$  and  $^4\text{He} + ^4\text{He}^{23}\text{Na}$  reaction processes. With weakly-bound molecules reacting with atoms at very low colliding energies, we interpret our results on the light of Efimov physics which supports model independence and robustness of our predictions. Specific sensitivities on the effective range were evidenced, highlighted by the particular inversion role of the  $p$ - and  $d$ -waves in the atom exchange and dissociation processes.

## I. INTRODUCTION

The fast development of methods to control atom and molecules in ultra-cold experiments, which have followed after the realization that Feshbach resonance techniques [1] could be used to manipulate the two-body interaction [2–4], made possible to emerge ultra-cold chemistry as a new field of interest with an intense research activity in recent years. On this regard, some previous reviews can be found on collisions with ultra-cold atoms and related discussions on possible experimental investigations [5–8], which were followed by Ref. [9], where the basis are settled for investigations on collisions and reactions with ultracold molecules. This work [9], in which it was concluded that the magnitude of elastic collision cross sections depends more on the mass and symmetry than on the interaction, came just after the experimental realization of Bose-Einstein condensation of Cooper-paired molecules of  $^6\text{Li}_2$  [10] and  $^{40}\text{K}_2$  [11]. Inelastic molecule-molecule and molecule-atom collisions were also characterized within the study of dissociation and decay of ultra-cold sodium molecules driven by the Feshbach mechanism [12]. The investigations on ultra-cold molecules via Feshbach mechanism can be exemplified by recent production of  $^{23}\text{Na}^{87}\text{Rb}$  molecules reported in Ref. [13] and the more recent investigation on ultra-cold  $^{23}\text{Na}^{39}\text{K}$  ground-state molecules [14], which can provide conditions for fully controlled studies with ultra-cold molecular collisions. Furthermore, it was recently reported progress with extreme mass imbalanced Fermionic mixtures where for the first time was observed magnetic Feshbach resonances in  $^6\text{Li}$  and  $^{173}\text{Yb}$  ultra-cold atoms [15].

With the complex structure of molecules, new opportunities can also be opened for research, such as the realization of quantum fluids of bosons with anisotropic interactions, as well as quantum coherent chemistry by

considering atom-molecule conversions.

Some pioneer experimental investigations with trapped ultracold atom-molecule collisions have been reported in 2006, in Refs. [16, 17], by considering cesium (Cs) atoms in  $\text{Cs}_2$  molecules. These works are followed by experiments with molecular collisions with tunable halo dimers, exploring four-body processes with identical bosons [18], inelastic collision rates of  $p$ -wave  $^6\text{Li}_2$  molecules [19],  $\text{RbCs}$  molecule collisions with Rb and Cs atoms [20]. Applications in cold controlled chemistry, with the possibilities to manipulate molecule collisions by electromagnetic fields, were discussed in Refs. [21–23], which together with references therein are covering both theoretical and experimental aspects in the first stages of investigations along these lines. As shown in these works, collisions of molecules with temperatures below 1 Kelvin can be manipulated by external electromagnetic fields. In Ref. [23], by considering potassium-rubidium molecules, it was also pointed out that, even when the cooled molecules have no energy to collide, exothermic atom exchange reactivity processes can occur through quantum mechanical tunneling. Nowadays, the reported experimental setups are showing an increasing level of control on atomic and molecular states, as one can trace from ongoing experimental and theoretical investigations, which can be exemplified by Refs. [24–33]. For more recent experimental activities reported in the last five years, on ultracold atom-dimer collisions, by using tunable Feshbach resonances, we should also mention the Refs. [34–41].

Our study is also motivated by the interest on verifying manifestations of Efimov physics [42] in atomic reactions, following Ref. [43], which could support previous theoretical studies with three-body weakly-bound systems [44–52]. In particular, the existence of a weakly-bound excited state in helium was established in Ref. [48]. This matter was further investigated in the Efimov physics context in Refs. [53–64], motivated by

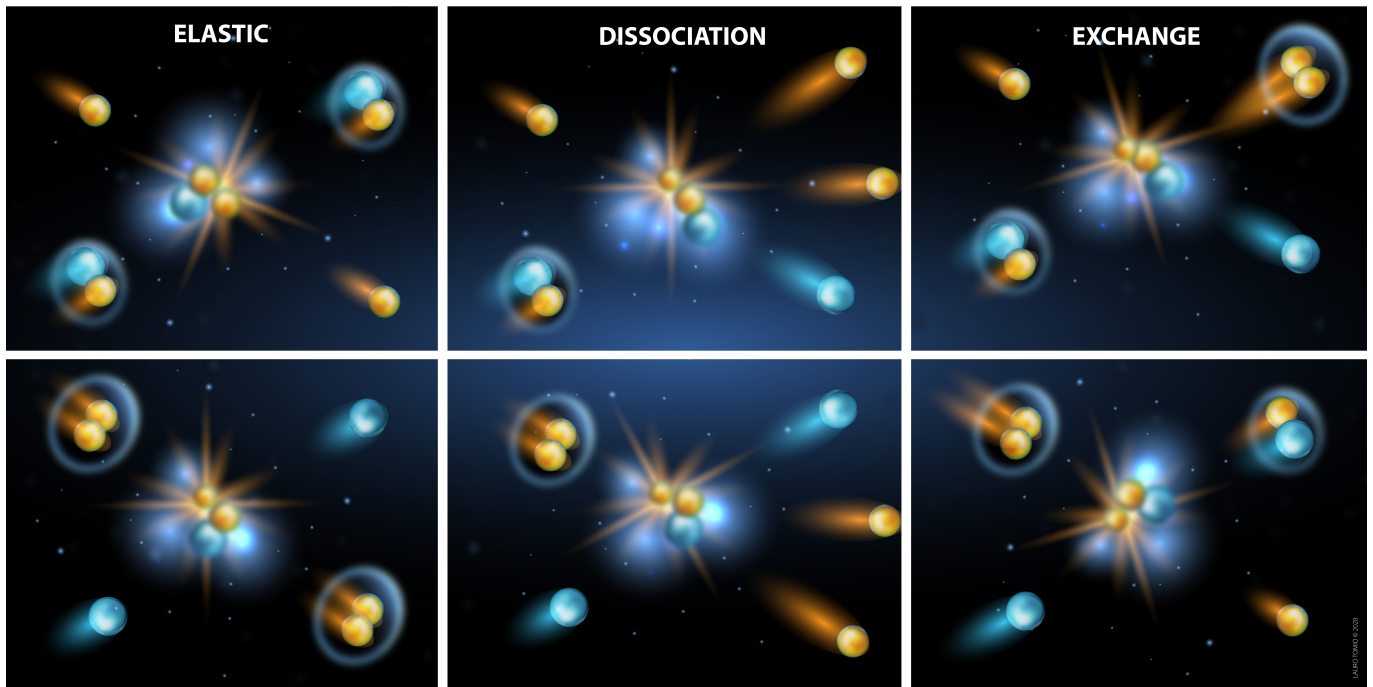


FIG. 1. Illustration of the atom-dimer reaction (for each panel, the entrance channel is in the left side, with the exit channel at the right side). The  $^4\text{He}$  is represented by the identical particles, with the dimers represented by  $^4\text{He}\beta$  ( $\beta = ^6\text{Li}, ^7\text{Li}$  or  $^{23}\text{Na}$ ) and  $^4\text{He}_2$  bound states. Assuming the  $^4\text{He}\beta$  is more bound than  $^4\text{He}_2$ , the atomic exchange reaction is endothermic in the upper-right panel; and exothermic in the lower-right one.

the remarkable small binding energy of the  $^4\text{He}$  dimer:  $B_{^4\text{He}_2} = 1.31$  mK, which was first reported independently in Refs. [65, 66], being more recently confirmed experimentally [67, 68]. The experimental success in verifying such long-time theoretical prediction, together with the results of previous experimental investigations of Efimov physics in cold atom laboratories [69–71], which are extended to mixed atomic-molecular combinations [72–75], became highly motivating for more deeper studies with single or mixed atomic species [76–81]. Quite remarkable are the advances in the laboratory techniques, such that one can even consider the possibility to alter the two-body interaction by using Feshbach resonance mechanisms (originally proposed in the nuclear physics context) [3]. The possibility of tuning the two-body scattering length in ultracold atomic experiments can alter in an essential way the balance between the non-linear first few terms of the mean-field description, as it was explored when modeling the atomic Bose-Einstein condensation [82].

The above mentioned experimental possibilities in cold chemistry laboratories and the interest to find further manifestations of the universal Efimov physics, motivate our study focusing on dissociation and atom exchange reactions with weakly-bound atom-molecular systems. Our aim is to explore the associated universal properties, which emerge in the studies of the reaction mechanisms of cold atoms with weakly-bound molecules. By following a previous investigation on  $s$ -wave scattering properties with the atomic species  $^4\text{He}$ ,  $^6\text{Li}$ ,  $^7\text{Li}$  and

$^{23}\text{Na}$  [43], with our present study we are providing a detailed analysis on atom-dimer dissociation and exchange reactions, in which we discuss and quantify the  $s$ ,  $p$  and  $d$  lower partial-wave contributions to the associated reaction rates. The choice of these four atomic samples relies on the fact that the dimer and trimer binding energies are enough known, either from available realistic potential model calculations or from experiments as in the case of  $^4\text{He}_2$ , which provide support to our theoretical predictions. In this introduction we are including a pictorial illustration of the reactions that we are considering (see Fig. 1), by assuming the common case in which the  $^4\text{He}\beta$  molecule ( $\beta = ^6\text{Li}, ^7\text{Li}$  or  $^{23}\text{Na}$ ) is more bound than the  $^4\text{He}_2$  dimer. For the entrance channel, in the upper row of this illustration we have the collision of a single  $^4\text{He}$  atom with the  $^4\text{He}\beta$  molecule; in the lower row, the single  $\beta$  atom collides with the  $^4\text{He}_2$  dimer.

In the present work, the Faddeev formalism was adopted [83] with renormalized zero-range (ZR) [84] and finite-range Yamaguchi [85] separable (FR) two-body interactions, using as inputs the available results reported in Ref. [86] for the dimer and trimer binding energies obtained from realistic interactions. These realistic interaction binding energies reported in Ref. [86] are selected from different potential models discussed in the literature, being guided by the corresponding available experimental results.

In the next Sect. II, we present the basic three-body formalism for two-atom mixtures, in which our main focus is on the case of atom-dimer collision, for separable

two-body interactions. Details on reaction rates and existent models are presented in Sect. III. In the next three sections (IV, V and VI) we have separated the corresponding results for the mixtures of  $^4\text{He}$  with  $^6\text{Li}$ ,  $^7\text{Li}$  and  $^{23}\text{Na}$ , respectively. Our final remarks and conclusions are presented in Sect. VII. In addition, three appendices are added to detail the three-body framework.

## II. THREE-BODY FRAMEWORK

The standard Faddeev formalism for three-body systems [83, 87, 88] with two atomic species interacting through one-term separable potentials including the zero-range one is presented in this section, by considering the elastic and rearrangement scattering amplitudes, from the collision of one of the atoms with a dimer formed by the remaining ones. (The detailed derivation of the scattering equations are presented in Appendix A.) As explained in our motivation for this study (with three-body system having two distinct atoms), we choose the identical two particles, labelled  $\alpha$ , as the  $^4\text{He}$  atom, with the third atom, labelled  $\beta$ , being  $^7\text{Li}$ ,  $^6\text{Li}$ , or  $^{23}\text{Na}$ . This particular choice is related to the available data obtained from experimental and well-known potential models for the three-body and two-body binding energies, when assuming different combinations of the corresponding three-particle atom-dimer systems. Our motivation also relies on the actual interest in the production of ultracold molecular systems [13, 14], and in the recent investigations on binary molecular collisions [34–36, 38, 40], together with experimental studies with these atomic samples [33, 41].

In this study, we assume that the selected three-body system ( $\alpha\alpha\beta$ ) is always bound, as well as the possible subsystems ( $\alpha\beta$ ) and ( $\alpha\alpha$ ), with the corresponding available data being used as inputs coming from different realistic potential models (given by previous available studies), together with existent experimental data. So, we assume as fixed the  $^4\text{He}_2$  binding energy and corresponding scattering length, such that  $E_{\alpha\alpha} = -B_{\alpha\alpha} = -1.31\text{mK}$  and  $a_{\alpha\alpha} = 100\text{\AA}$ . For the other input binding energies, we select two specific models which have been discussed in Ref. [43], that we found enough representative to explore the sensibility of our results on dimer binding energies variation. As it will be discussed, by using different potential models, we expect our results on reaction rates, together with possible future experimental data, be useful in selecting the appropriate two-body potential model.

### A. Bound-state $\alpha\alpha\beta$ three-body system

We start by recovering some details from Ref. [43], in order to fix the notation of the formalism, summarizing the  $s$ -wave three-body bound-state coupled equation when considering separable potentials with all sub-

systems being bound. We assume units such that  $\hbar = 1$  (with energies given in mK), with  $m \equiv m_\alpha = m_{^4\text{He}}$  and a mass ratio defined by  $A \equiv m_\beta/m_\alpha$ . So, for the reduced masses we have  $\mu_{\alpha\alpha} = m/2$  and  $\mu_{\alpha\beta} = Am/(A+1)$  for the  $\alpha\alpha$  and  $\alpha\beta$  subsystems, respectively. The corresponding three-body reduced masses are given by  $\mu_{\alpha(\alpha\beta)} = m(A+1)/(A+2)$  for the  $\alpha - (\alpha\beta)$ ; and  $\mu_{\beta(\alpha\alpha)} = m(2A)/(A+2)$  for the  $\beta - (\alpha\alpha)$ . The bound-state energies for the two- and three-body systems are given by  $E_{\alpha\alpha} \equiv -B_{\alpha\alpha}$ ,  $E_{\alpha\beta} \equiv -B_{\alpha\beta}$  and  $E_3 \equiv -B_3$ , respectively; with the energies of the  $s$ -wave elastic colliding particle given by  $E_{k_\alpha} \equiv k_\alpha^2/[2\mu_{\alpha(\alpha\beta)}] \equiv E_3 - E_{\alpha\beta}$  and  $E_{k_\beta} \equiv k_\beta^2/[2\mu_{\beta(\alpha\alpha)}] \equiv E_3 - E_{\alpha\alpha}$ . The extension to higher partial waves will be done along the following subsection. In this case, the Faddeev coupled equations are reduced to integral equations for the momentum space spectator functions of the particles  $\alpha$  and  $\beta$ , which are given by  $\chi_\alpha(\mathbf{q}; E_3)$  and  $\chi_\beta(\mathbf{q}; E_3)$ . Considering the  $s$ -wave case, by redefining these functions, as  $\chi_{j=\alpha,\beta}(q; E_3) \equiv \bar{\chi}_j(q; E_3)/(q^2 + |k_j^2|)$ , the corresponding coupled formalism is given by

$$\bar{\chi}_\alpha(q; E_3) = \bar{\tau}_\alpha(q; E_3) \int_0^\infty dk k^2 \left[ K_2^0(q, k; E_3) \frac{\bar{\chi}_\alpha(k; E_3)}{(k^2 + |k_\alpha^2|)} + K_1^0(q, k; E_3) \frac{\bar{\chi}_\beta(k; E_3)}{(k^2 + |k_\beta^2|)} \right], \quad (1)$$

$$\bar{\chi}_\beta(q; E_3) = \bar{\tau}_\beta(q; E_3) \int_0^\infty dk k^2 K_1^0(k, q; E_3) \frac{\bar{\chi}_\alpha(k; E_3)}{(k^2 + |k_\alpha^2|)},$$

where  $K_1^0(q, k; E_3)$  and  $K_2^0(q, k; E_3)$  are the appropriate momentum space kernels, which will be explicitly given according to the kind of form-factors one considers for the two-body interaction. The respective two-body  $t$ -matrix elements for the  $\alpha\beta$  and  $\alpha\alpha$  bound subsystems are  $\bar{\tau}_\alpha(q; E_3)$  and  $\bar{\tau}_\beta(q; E_3)$ , in which  $\bar{\tau}_j$  and the  $s$ -wave kernels  $K_{1,2}^0$  will be appropriately extended to  $\ell$  partial waves in the Appendix B, when considering the specific potential models.

### B. Atom-dimer collision

By considering atom-dimer collision with two different atomic species, we have three separate channels in the continuum: elastic scattering, rearrangement (exchange reaction), and breakup (dissociation reaction). For the scattering of  $\alpha$  by the  $\alpha\beta$  bound subsystem, by using the symmetry properties applied to identical bosons, the  $\ell$ -partial-wave scattering amplitudes,  $h_\alpha^\ell$  and  $h_\beta^\ell$ , with one-term separable potentials, can be written as follows (see Appendices A and B):

$$h_\alpha^\ell(q; E_3) = \bar{\tau}_\alpha(q; E_3) \left\{ \frac{\pi}{2} K_2^\ell(q, k_\alpha; E_3) + \int_0^\infty dk k^2 \right. \quad (2) \\ \left. \times \left[ K_2^\ell(q, k; E_3) \frac{h_\alpha^\ell(k; E_3)}{(k^2 - k_\alpha^2 - i\epsilon)} + K_1^\ell(q, k; E_3) \frac{h_\beta^\ell(k; E_3)}{q^2 - k_\beta^2 - i\epsilon} \right] \right\},$$

$$h_\beta^\ell(q; E_3) = \bar{\tau}_\beta(q; E_3) \left\{ \frac{\pi}{2} K_1^\ell(k_\alpha, q; E_3) + \int_0^\infty dk k^2 K_1^\ell(k, q; E_3) \frac{h_\alpha^\ell(k; E_3)}{(k^2 - k_\alpha^2 - i\epsilon)} \right\}, \quad (3)$$

where  $k_\alpha$  and  $k_\beta$  are the on-shell momenta (already defined), with  $h_\alpha^\ell(k_\alpha; E_3)$  representing the on-shell elastic amplitude and  $h_\beta^\ell(k_\alpha; E_3)$  the corresponding on-shell atom-exchange amplitude.  $K_{1,2}^\ell$  which have been introduced (for  $\ell = 0$ ) in Eq. (1) are momentum space kernels in  $\ell$ -wave. From the scattering amplitudes, we can obtain the cross sections with the corresponding reaction rates. For the elastic scattering, we obtain (see Appendix C)

$$\sigma_{el}(E_{k_\alpha}) = 4\pi \sum_\ell (2\ell + 1) |h_\alpha^\ell(k_\alpha; E_3)|^2, \quad (4)$$

with the exchange reaction cross section given by

$$\sigma_{ex}(E_{k_\alpha}) = \frac{2\pi f_\alpha^2}{f_\beta^2} \sqrt{\frac{\mu_{\alpha(\alpha\beta)}}{\mu_{\beta(\alpha\alpha)}}} \left( 1 - \frac{E_{\alpha\alpha} - E_{\alpha\beta}}{E_{k_\alpha}} \right) \times \sum_\ell (2\ell + 1) |h_\beta^\ell(k_\alpha; E_3)|^2, \quad (5)$$

where the on-shell  $h_\alpha^\ell$  and  $h_\beta^\ell$  are obtained from Eqs. (2) and (3).

For the scattering of particle  $\beta$  by the  $\alpha\alpha$  bound subsystem, the scattering amplitudes can be calculated by the following coupled equation (see Appendices A and B):

$$h_\alpha^\ell(q; E_3) = \bar{\tau}_\alpha(q; E_3) \left\{ \pi K_1^\ell(q, k_\alpha; E_3) + \int_0^\infty dk k^2 \right. \quad (6)$$

$$\times \left[ K_2^\ell(q, k; E_3) \frac{h_\alpha^\ell(k; E_3)}{(k^2 - k_\alpha^2 - i\epsilon)} + K_1^\ell(q, k; E_3) \frac{h_\beta^\ell(k; E_3)}{q^2 - k_\beta^2 - i\epsilon} \right] \Big\},$$

$$h_\beta^\ell(q; E_3) = \bar{\tau}_\beta(q; E_3) \int_0^\infty dk k^2 K_1^\ell(k, q; E_3) \frac{h_\alpha^\ell(k; E_3)}{(k^2 - k_\alpha^2 - i\epsilon)}. \quad (7)$$

Here  $h_\alpha^\ell$  represents the exchange reaction and  $h_\beta^\ell$  represents the elastic scattering. In this case elastic and exchange reaction cross sections can be calculated by (see Appendix C):

$$\sigma_{el}(E_{k_\beta}) = \pi \sum_\ell (2\ell + 1) |h_\beta^\ell(k_\beta; E_3)|^2, \quad (8)$$

and

$$\sigma_{ex}(E_{k_\beta}) = \frac{2\pi f_\beta^2}{f_\alpha^2} \sqrt{\frac{\mu_{\beta(\alpha\alpha)}}{\mu_{\alpha(\alpha\beta)}}} \sqrt{1 - \frac{E_{\alpha\beta} - E_{\alpha\alpha}}{E_{k_\beta}}} \times \sum_\ell (2\ell + 1) |h_\alpha^\ell(k_\beta; E_3)|^2, \quad (9)$$

where the on-shell  $h_\alpha^\ell(k_\beta)$  and  $h_\beta^\ell(k_\beta)$  are calculated from Eqs. (6) and (7). The  $f_\alpha$  and  $f_\beta$  factors, together with detailed derivation of the scattering amplitudes and cross sections for each potential, are described in the Appendix C.

The scattering amplitude for breakup or dissociation reaction can also be calculated by the summation over half-off-shell results of  $h_\alpha$  and  $h_\beta$  using the Eqs. (2) and (3) (for  $\alpha - \alpha\beta$  scattering) and by using Eqs. (6) and (7) (for  $\beta - \alpha\alpha$  scattering). The breakup amplitude is not detailed in the presented work. However, the dissociation rate is obtained through the inelasticity parameter of the elastic amplitude and rearrangement rate, as explained in the following section.

### III. REACTION RATES AND MODELS

The reaction rates are defined in terms of the product of the corresponding cross sections (which are detailed in the Appendix C) and the respective velocity of the colliding particle. By assuming that the atom-dimer reaction has initially the particle  $\alpha$  or  $\beta$  colliding with the dimer formed by the particles  $\alpha\beta$  or  $\alpha\alpha$ , respectively, with energy  $E_k \equiv k^2/(2\mu)$ , with  $\mu$  being the atom-dimer reduced mass, the total elastic case is such that  $\alpha + \alpha\beta \rightarrow \alpha + \alpha\beta$  or  $\beta + \alpha\alpha \rightarrow \beta + \alpha\alpha$ . Therefore, the elastic reaction rate is given by corresponding product of the elastic cross section with the velocity  $\hbar k/\mu$ , such that

$$K_{\text{elas}}(E_k) = \frac{\hbar k}{\mu} \sigma_{\text{el}}(E_k). \quad (10)$$

Analogously, the atom-exchange reaction rate can be defined, corresponding to the processes  $\alpha + \alpha\beta \rightarrow \beta + \alpha\alpha$  (or  $\beta + \alpha\alpha \rightarrow \alpha + \alpha\beta$ ), which is given by

$$K_{\text{ex}}(E_k) = \frac{\hbar k}{\mu} \sigma_{\text{ex}}(E_k). \quad (11)$$

The third possible process refers to dissociation processes (possible for energies above the three-body continuum), when for example  $\alpha + \alpha\beta \rightarrow \alpha + \alpha + \beta$ . It is given by

$$K_{\text{diss}}(E_k) = \frac{\hbar k}{\mu} \sigma_{\text{diss}}(E_k). \quad (12)$$

Given the above, in terms of the corresponding cross-sections, we define the loss-rate coefficient by

$$K_{\text{loss}}(E_k) = K_{\text{ex}}(E_k) + K_{\text{diss}}(E_k). \quad (13)$$

which refers to the exchange and dissociation, or breakup, cross-sections, respectively.

As in our approach we have two different initial configurations for two-identical particles  $\alpha$  with a particle  $\beta$ , the above defined quantities (momentum  $k$ , energy  $E_k$  and reduced mass  $\mu$ ) should be understood such that: (i) If  $\alpha$  is the colliding particle,  $k \equiv k_\alpha$ ,  $E_k \equiv E_{k_\alpha}$  and  $\mu \equiv \mu_{\alpha(\alpha\beta)} = m_\alpha(m_\alpha + m_\beta)/(2m_\alpha + m_\beta)$ ; (ii) if  $\beta$  is the colliding particle,  $k \equiv k_\beta$ ,  $E_k \equiv E_{k_\beta}$  and  $\mu \equiv \mu_{\beta(\alpha\alpha)} = (2m_\beta m_\alpha)/(2m_\alpha + m_\beta)$ .

The corresponding partial wave  $\ell$  decomposition of the above reaction rates [Eqs. (10) - (13)] can be expressed in terms of the non-diagonal S-matrix, for the elastic and for

the atom-exchange channel. Given that  $K_x(E_k) \equiv K_x$ , for  $x = (\text{elas}, \text{ex}, \text{diss}, \text{loss})$ , we have the following:

$$K_{\text{elas}} = \frac{\pi\hbar}{\mu k} \sum_{\ell=0}^{\infty} (2\ell+1) |1 - S_{\text{el}}^{\ell}(E_k)|^2, \quad (14)$$

$$K_{\text{ex}} = \frac{\pi\hbar}{\mu k} \sum_{\ell=0}^{\infty} (2\ell+1) |S_{\text{ex}}^{\ell}(E_k)|^2, \quad (15)$$

$$K_{\text{diss}} = \frac{\pi\hbar}{\mu k} \sum_{\ell=0}^{\infty} (2\ell+1) (1 - |S_{\text{el}}^{\ell}(E_k)|^2 - |S_{\text{ex}}^{\ell}|^2), \quad (16)$$

$$K_{\text{loss}} = \frac{\pi\hbar}{\mu k} \sum_{\ell=0}^{\infty} (2\ell+1) (1 - |S_{\text{el}}^{\ell}(E_k)|^2). \quad (17)$$

Our aim is to study the reaction rates for the atom-dimer collisions, in which  $\alpha \equiv {}^4\text{He}$ , with  $\beta \equiv {}^6\text{Li}$ ,  ${}^7\text{Li}$ , and  ${}^{23}\text{Na}$ , by considering all possible combinations for the three  $\alpha\alpha\beta$  systems. The relevant information about these systems are provided in Tables I and II, with the dimer and trimer binding energies being obtained from Refs. [86] (a1) and [49] (a2). The respective configuration-space behaviors of the two-body potentials  $V(r)$ , which were used to obtain the dimer energies provided in Refs. [49] and [86], are represented in Fig. 2.

The corresponding two- and three-body ground-state binding energies (absolute values, given in mK) are presented in Table I, in which we also include the given excited three-body binding energies, whenever known. More specifically, the results for (a1) and (a2) were obtained by considering interactions from Refs. [89] and [90], respectively, as shown in Fig. 2. Other model calculations exist for the systems we are studying, beyond the selected (a1) and (a2) models, as described in Ref. [86]. They are from Ref. [60], with  $\alpha\alpha$  and  $\alpha\beta$  potentials given by Refs. [89, 91]; from Ref. [59, 60], with potentials given by Ref. [93, 94]; from Ref. [62], with  $\alpha\alpha$  potential given by Ref. [93], and  $\alpha\beta$  by Ref. [89]. However, we select only (a1) and (a2), among the ones which are discussed in Refs. [43, 86], as they are providing values for all the cases we are considering, having binding energies enough distinct for a significant comparative study.

One should notice that the binding-energy difference between the dimers  ${}^4\text{He}-{}^6\text{Li}$  and  ${}^4\text{He}-{}^7\text{Li}$ , shown in Table I, refers to the corresponding isotopic mass difference. More relevant to be noticed in the table, for such weakly-bound systems, is the binding energy sensibility on the potential depth differences, as verified between the (a1) and (a2) models for the He-Li system (see the inset of Fig. 2), which changes the kind of the atom-exchange reaction (endothermic or exothermic).

The Table II refers to the kind of each reaction channel considered in the two potential models we have used (ZR and FR) with both different inputs. In all the cases under our analysis, in which we have two  ${}^4\text{He}$  atoms, identified by  $\alpha$  and a third atom identified by  $\beta = ({}^6\text{Li}, {}^7\text{Li}, {}^{23}\text{Na})$ , a weakly bound molecule exists, such that six entrance channels are possible for the atom-dimer reactions, which are the following:

$$\left. \begin{array}{l} (1) \quad {}^4\text{He} + {}^4\text{He}^6\text{Li}, \\ (2) \quad {}^6\text{Li} + {}^4\text{He}_2, \\ (3) \quad {}^4\text{He} + {}^4\text{He}^7\text{Li}, \\ (4) \quad {}^7\text{Li} + {}^4\text{He}_2, \\ (5) \quad {}^4\text{He} + {}^4\text{He}^{23}\text{Na}, \\ (6) \quad {}^{23}\text{Na} + {}^4\text{He}_2. \end{array} \right\} \quad (18)$$

For each one of these atom-dimer initial reaction channels,

we can obtain the elastic, atom exchange and dissociation reaction rates. In order to compute these quantities, among the available potential models which were investigated in Refs. [49, 86], we select two of them, as we already mentioned, which provide less-similar values for the dimer and trimer binding energies that we are considering. These potential models will be used to provide the necessary binding energies for the inputs to adjust the parameters of our zero-range and finite-range  $s$ -wave separable interactions, within a Faddeev three-body formalism for the atom-dimer collision (for details, see sect. II B).

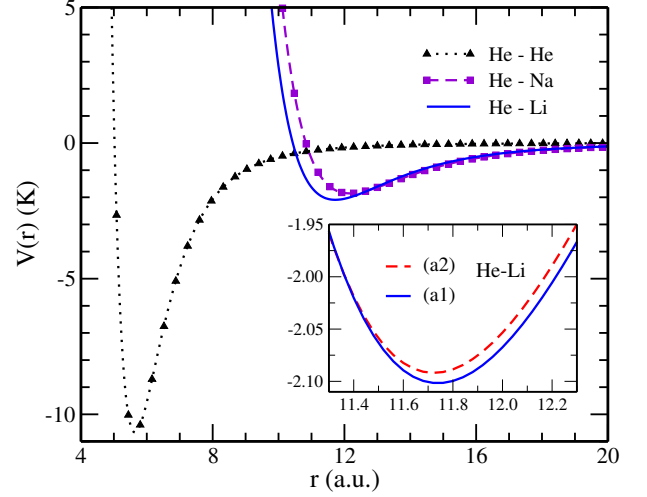


FIG. 2. Dimer potentials for the He-He (dotted-line with triangles), He-Na (dashed-line with squares) and He-Li (solid line) systems, used in the three-body calculations of [86] (a1) and [49] (a2), are shown in the main frame. The He-Li (a1) and (a2) potentials, respectively derived in Refs. [89] and [90], differ by tenth's of mK, being indistinguishable and represented by a single line in the main frame. They are shown in the inset by the solid (a1) and dashed (a2) lines.

TABLE I. This table provides the available dimer and trimer binding energies (in mK), combining two  ${}^4\text{He}$  with  ${}^6\text{Li}$ ,  ${}^7\text{Li}$  and  ${}^{23}\text{Na}$  atoms. The given results for (a1) are from Ref. [86] and for (a2) from [49]. With (\*) we have the available excited binding energies, from Ref. [86].

Molecule	(a1)	(a2)
${}^4\text{He}_2$	1.31	1.31
${}^4\text{He}^6\text{Li}$	1.515	0.12
${}^4\text{He}^7\text{Li}$	5.622	2.16
${}^4\text{He}^{23}\text{Na}$	28.98	28.98
${}^4\text{He}_2-{}^6\text{Li}$	57.23	31.4
$({}^4\text{He}_2-{}^6\text{Li})^*$	1.937	-
${}^4\text{He}_2-{}^7\text{Li}$	79.36	45.7
$({}^4\text{He}_2-{}^7\text{Li})^*$	5.642	-
${}^4\text{He}_2-{}^{23}\text{Na}$	150.9	103.1

In order to compute the reaction rates, as mentioned before, for each set of binding energies (a1) and (a2) provided in Table I, we have adjusted our zero-range and finite-range two-body interactions, for which the corresponding kernels of the

TABLE II. Classification of reaction channels, identified in (18), as endothermic or exothermic according to dimer binding energies of models (a1) and (a2), given in Table I, for elastic and exchange processes. For dissociation ( $\rightarrow {}^4\text{He} + {}^4\text{He} + {}^6\text{Li}$ ), all channels are endothermic.

Channel	Model	Elastic	Exchange
(1)		${}^4\text{He} + {}^4\text{He} + {}^6\text{Li}$	${}^4\text{He}_2 + {}^6\text{Li}$
	(a1)		endothermic
	(a2)		exothermic
(2)		${}^6\text{Li} + {}^4\text{He}_2$	${}^4\text{He} + {}^4\text{He} + {}^6\text{Li}$
	(a1)		exothermic
	(a2)		endothermic
(3)		${}^4\text{He} + {}^4\text{He} + {}^7\text{Li}$	${}^4\text{He}_2 + {}^7\text{Li}$
	(a1)		endothermic
	(a2)		endothermic
(4)		${}^7\text{Li} + {}^4\text{He}_2$	${}^4\text{He} + {}^4\text{He} + {}^7\text{Li}$
	(a1)		exothermic
	(a2)		exothermic
(5)		${}^4\text{He} + {}^4\text{He} + {}^{23}\text{Na}$	${}^4\text{He}_2 + {}^{23}\text{Na}$
	(a1)		endothermic
	(a2)		endothermic
(6)		${}^{23}\text{Na} + {}^4\text{He}_2$	${}^4\text{He} + {}^4\text{He} + {}^{23}\text{Na}$
	(a1)		exothermic
	(a2)		exothermic

scattering equations are detailed in Appendix B. In the zero range model, we have the two-body amplitude parametrized by the diatomic binding energies, together with a regularizing momentum parameter fixed by the triatomic molecule. For the finite-range interaction, we assume a rank-one separable Yamaguchi potential, given by

$$V_{ij}(p, p') = \lambda_{ij} \frac{1}{p^2 + \gamma_{ij}^2} \frac{1}{p'^2 + \gamma_{ij}^2}, \quad (19)$$

where  $ij = \alpha\alpha$  or  $\alpha\beta$ , respectively, for the  $\alpha\alpha$  or  $\alpha\beta$  two-body subsystems.  $\lambda_{ij}$  and  $\gamma_{ij}$  refer to the strengths and ranges of the respective two-body interactions. As in the present approach we consider only bound (negative) two-body subsystems,  $E_{ij} = -B_{ij}$ , the corresponding relations for the strengths and ranges are given by

$$\lambda_{ij}^{-1} = \frac{-2\pi\mu_{ij}}{\gamma_{ij}(\gamma_{ij} + \kappa_{ij})^2}, \quad r_{ij} = \frac{1}{\gamma_{ij}} + \frac{2\gamma_{ij}}{(\gamma_{ij} + \kappa_{ij})^2}, \quad (20)$$

where  $r_{ij}$  are the effective ranges, with

$$\kappa_{\alpha\alpha} \equiv \sqrt{-2\mu_{\alpha\alpha}E_{\alpha\alpha}}, \quad \kappa_{\alpha\beta} \equiv \sqrt{-2\mu_{\alpha\beta}E_{\alpha\beta}}. \quad (21)$$

For the case of FR potential given in Eq. (19), the parameters with corresponding ranges and scattering lengths, are shown in Table III, given in three blocks for the cases with ( ${}^4\text{He} + {}^7\text{Li}$ ), ( ${}^4\text{He} + {}^6\text{Li}$ ) and ( ${}^4\text{He} + {}^{23}\text{Na}$ ). We observe that, in all the cases, for the dimer  ${}^4\text{He}_2$  binding energy, the accepted value  $B_{\alpha\alpha} = 1.31$  mK is being considered, with the corresponding parameters given in this table.

The results for the reaction rates are organized according to the Table II and are calculated with the ZR and FR potential models, in order to exhibit the model independent features of

TABLE III. Parameters used in the FR  $s$ -wave separable interaction, with the corresponding ranges and scattering lengths, in order to reproduce the respective binding energies given in Table I for the model potentials (a1) and (a2).

Dimer	Model	$\gamma_{\alpha\beta}(\text{\AA}^{-1})$	$r_{\alpha\beta}(\text{\AA})$	$a_{\alpha\beta}(\text{\AA})$
${}^4\text{He} + {}^6\text{Li}$	(a1)	0.17	15.85	90.38
	(a2)	0.14	20.04	300.37
${}^4\text{He} + {}^7\text{Li}$	(a1)	0.17	14.77	50.08
	(a2)	0.14	19.02	77.43
${}^4\text{He} + {}^{23}\text{Na}$	(a1)	0.16	12.44	25.34
	(a2)	0.09	19.0	34.24
${}^4\text{He}_2$	(a1)&(a2)	0.39	7.34	100

the present results, for up to the  $d$ -wave contribution. The choice of the potential, ZR or FR, affects mainly the  $s$ -wave contribution, which is more sensitive to the effective range. Reminding that the models fit the same diatomic and triatomic binding energies, we found that the bulk results are almost model independent; particularly, for the higher partial waves the results are to a large extend universal. Such features gives robust outcomes of our model calculations, as we will present in the following. However, the reaction rates are bounded by the binding energies provided in Refs. [86] and [49], while our predictions allow to discriminate between the very different values given for the model (a1) and (a2). We perform calculations up to kinetic energies of 0.1 K. Note also that, we have carefully checked that almost no deviation from the unitarity appears in our numerical solutions of the scattering equations, for all the colliding energies being considered. In particular, we verified that the coupled elastic and atom-exchange channels S-matrix is unitary below the dissociation threshold, as obtained numerically for both zero- and finite-range interaction models.

TABLE IV. For the molecules identified in the first column, in the 2nd, 3rd and 4th columns we have the corresponding two-body energies (mK), scattering lengths ( $\text{\AA}$ ), and trimer energies (mK) (obtained from Ref. [86]), respectively. In the 5th to 7th columns we have the first excited bound-state energies (in mK). Results obtained from Refs. [86] and [43], as indicated in the last row. In addition, for the excited states, we show results obtained by using zero-range (ZR) and finite-range (FR) one-term separable interactions. The parameters for the  ${}^4\text{He}$ - ${}^4\text{He}$  subsystem are given in Tables I and III.

molecule	He-Li	$a_{\text{HeLi}}$	$\text{He}_2\text{Li}$	$(\text{He}_2\text{Li})^*$	$(\text{He}_2\text{Li})^*$	$(\text{He}_2\text{Li})^*$
${}^4\text{He}_2$ - ${}^6\text{Li}$	1.515	100	57.23	1.937	1.901	1.977
${}^4\text{He}_2$ - ${}^7\text{Li}$	5.622	48.84	79.36	5.642	-	5.672
Ref.	[86]	[43]	[86]	[86]	(ZR) [43]	(FR) [43]

Before closing this section, it is necessary to point out that the molecules  ${}^4\text{He}_2 + {}^6\text{Li}$  and  ${}^4\text{He}_2 + {}^7\text{Li}$  present excited Efimov states close to the lowest scattering thresholds as verified in Ref. [86] and for the ZR and FR potentials in [43]. These results corresponding to model (a1) are provided in Table IV, where in [43] slightly different scattering lengths were used with respect to Table III, which is not relevant. It is important to note that weakly bound triatomic states close to the



threshold affect the reaction rates at low energies.

In what follows we will present our results for the atom-dimer reaction rates by considering the possible three-atom systems  $\alpha\alpha\beta$  with the particle  $\alpha$  being  ${}^4\text{He}$  and  $\beta$  being one of the species  ${}^6\text{Li}$ ,  ${}^7\text{Li}$  or  ${}^{23}\text{Na}$ . We split the presentation in the next three sections: In Sect. IV we consider  $\beta \equiv {}^6\text{Li}$ ; in Sect. V,  $\beta \equiv {}^7\text{Li}$ ; and in Sect. VI,  $\beta \equiv {}^{23}\text{Na}$ . In each of these three sections, we have two subsections for the reaction-rate results, such that  $\alpha + \alpha\beta$  reactions are presented in (A), with the  $\beta + \alpha\alpha$  reactions presented in (B), with all the possibilities being presented in Table II.

#### IV. THREE BODY REACTIONS WITH HELIUM-4 AND LITHIUM-6

##### A. Reaction rates for ${}^4\text{He} + {}^4\text{He}^6\text{Li}$

The calculations for the reaction rates, i.e., elastic, exchange and loss, for the  ${}^4\text{He} + {}^4\text{He}^6\text{Li}$  collision are shown in the following. The parameters of the zero-range and rank-1 separable  $s$ -wave potential (see Table II) models are fitted to reproduce the binding energies obtained from the choices of potentials models given in Table I. The results are presented in Fig. 3 for model (a1) and in 4 for model (a2), and in each figure the outcome of the zero-range and separable finite range potential are shown.

The exchange and loss rates for the  ${}^4\text{He} + {}^4\text{He}^6\text{Li}$  with model (a1), shown in Fig. 3, correspond to endothermic reactions: the threshold energy in order to open the exchange channel is 0.2 mK, with the three-body dissociation at 1.5 mK. The  $s$ -wave elastic rate is dominant below opening the threshold attaining values as large as  $10^{-9}\text{cm}^3/\text{s}$ , for both the zero-range and finite-range potentials. Once the atom exchange channel opens, i.e.  ${}^4\text{He} + {}^4\text{He}^6\text{Li} \rightarrow {}^4\text{He}_2 + {}^6\text{Li}$ , the  $p$ -wave becomes noticeable and right away gives the major contribution to both the atom exchange and loss rate, even above the dissociation channel.

The  $p$ -wave dominance comes from the well-known one-atom exchange diagram, which due to the involved small binding energy has a pole close to the scattering threshold. Physically in the exchange process, the incoming  ${}^4\text{He}$  picks the other one from the  ${}^4\text{He}^6\text{Li}$  molecule, and the remaining  ${}^6\text{Li}$  is moving backwards with respect to the incoming  ${}^4\text{He}$ , enhancing the  $p$ -wave contribution to the reaction process.

The  $s$ -wave projection of the one-atom exchange diagram is also associated with the appearance of the Efimov effect, as such diagram comes also as the kernel of the integral equations for the scattering and bound state, both for the zero-range and separable potential models. One can observe that both models predict very similar reaction rates, as these low-energy process are quite universal, and determined by the two-atoms low energy observables (in this case the binding energies) and one three-body input, as the binding energies of the triatomic molecules. The separable interaction model has indeed scattering lengths almost three times the effective ranges (see Table II), characterizing well a short range potential with three-body low energy observables weakly dependent on the range. It is important to emphasize that the  $s$ -wave observables are more sensitive to the potential, as they require for the limit of zero-range interaction the information of the triatomic binding energy, while the  $p$ ,  $d$ , .... waves

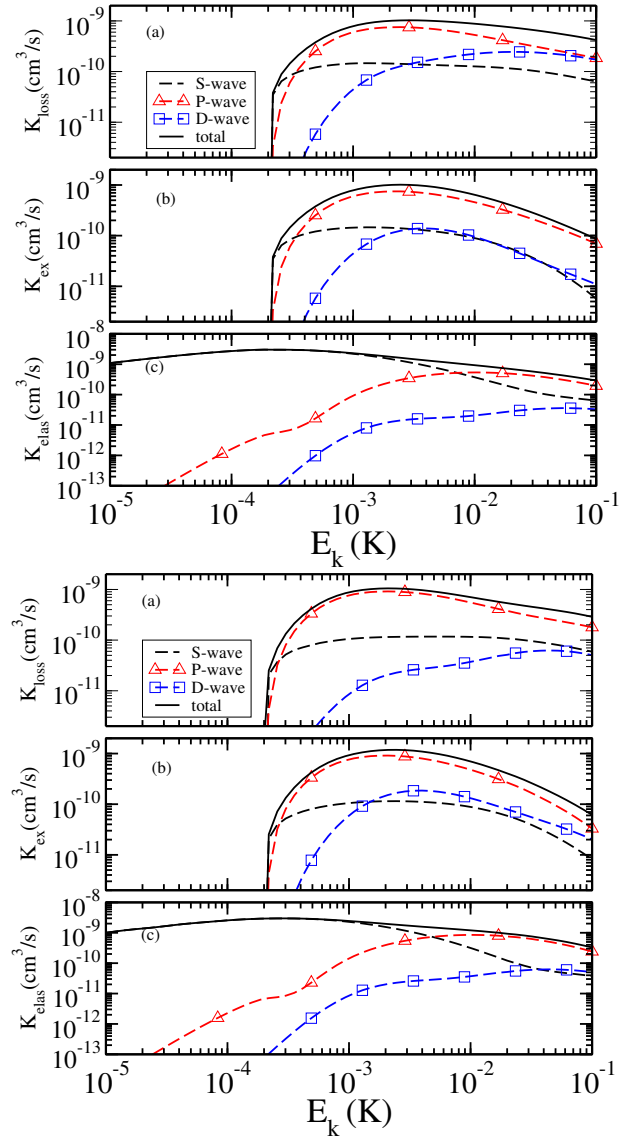


FIG. 3. Reaction rates for  ${}^4\text{He} + {}^4\text{He}^6\text{Li}$ , using zero-range (upper-set of panels) and finite-range (lower-set of panels) interactions, considering the (a1) model.

are essentially sensitive to the on-shell low energy two-atom amplitude.

The reaction rates for  ${}^4\text{He} + ({}^4\text{He}^6\text{Li})$  obtained with model (a2) are shown in Fig. 4. Now, the atom exchange reaction is exothermic (see Table III), with the three-atom continuum opening at 0.12mK. The  $s$ -wave is dominant up to this threshold with rates above  $10^{-9}\text{cm}^3/\text{s}$ . The  $s$ -wave elastic rate has a minimum at the inelastic threshold, with the  $p$ -wave emerging as the dominant one above it. The  $d$ -wave is in general less important, but can be comparable with the  $s$ -wave for higher energies. The manifestation of the minimum in the  $s$ -wave can be clearly seen in the elastic rate. The  $d$ -wave phase shift has also a zero around 1mK, reflected as a minimum of the elastic amplitude, due to the absorption. This feature is model independent, as one can observe by comparing the two potential models. The atom exchange rate is dominated by the  $p$ -wave above the dissociation threshold, with the  $s$ - and  $d$ -waves representing less than 20% of the rate. The calculated loss rate for the reaction  ${}^4\text{He} + {}^4\text{He}^6\text{Li}$  is

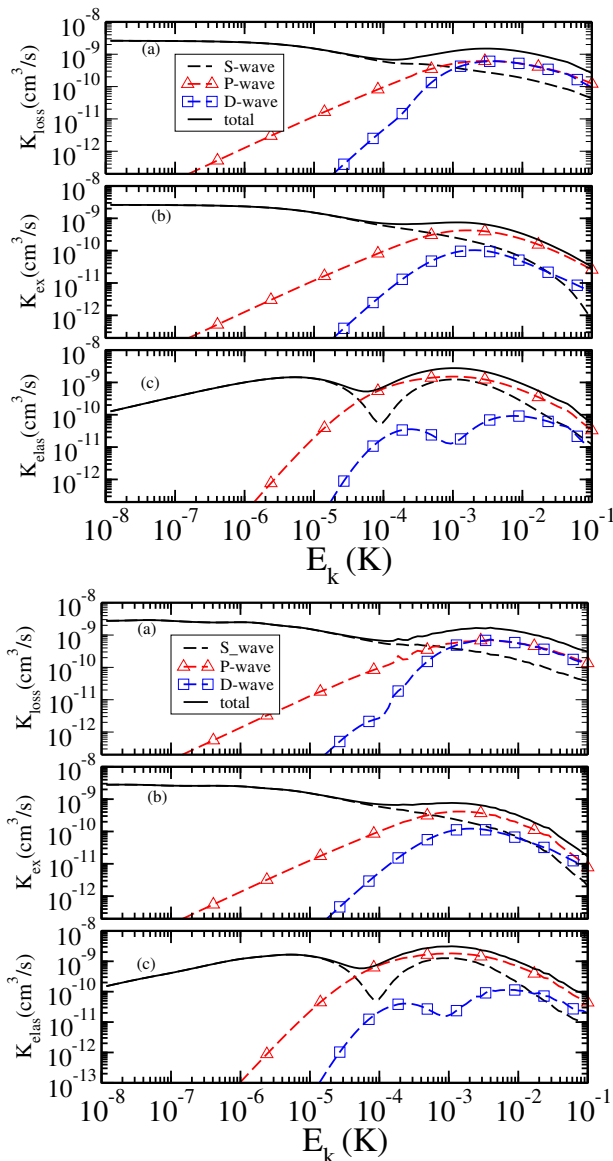


FIG. 4. Reaction rates for  ${}^4\text{He} + {}^4\text{He}^6\text{Li}$ , using zero-range (upper-set of panels) and finite-range (lower-set of panels) interactions, considering the (a2) model.

also shown in Fig. 4 for the model (a2). A noticeable dip appears at 0.1 mK, which comes from the fast increase of the  $p$ - and  $d$ -waves contribution to the dissociation channel, while the  $s$ -wave becomes less relevant. The dissociation channel is more efficiently populated by the higher partial waves, as the relevant inputs are only the binding energies of the  ${}^4\text{He}$  dimer and the  ${}^4\text{He}^6\text{Li}$ , which in this case are pretty small.

As already mentioned, beyond  $s$ -wave the three-body scattering amplitudes are dominated by the on-shell two-atom low-energy T-matrix, which sizes the kernel of the three-body scattering equation as can be clearly verified, for example, in the zero-range model. In this way, the bound state pole of the very weakly bound  ${}^4\text{He}^6\text{Li}$  molecule enhances even more the kernel and together the contribution of the  $p$ - and  $d$ -waves to the loss rate. The elastic, atom exchange and loss rates clearly distinguish the models (a1) and (a2), providing a mean to indirectly access the on-shell quantities. The difference in the binding energy of the  ${}^4\text{He}_2^6\text{Li}$  molecule in models (a1) and

(a2) is relevant for the  $s$ -wave, while it is barely perceived by the  $p$ - and  $d$ -waves, that show sensitivity to the different values of the  ${}^4\text{He}^6\text{Li}$  energy even above the dissociation threshold.

## B. Reaction rates for ${}^6\text{Li} + {}^4\text{He}_2$

The results for the reaction rates in the  ${}^6\text{Li} + {}^4\text{He}_2$  collision are shown in Figs. 5 and 6, with the  ${}^6\text{Li} + {}^4\text{He}_2 \rightarrow {}^4\text{He} + {}^4\text{He}^6\text{Li}$  reaction being exothermic for model (a1) and endothermic for model (a2) (see Table III). For the potential model (a1), the dissociation channel opens at 1.3 mK, dominating the losses only above 10 mK, as one can observe from the corresponding panels of Fig. 5. The elastic rate is dominated by the  $s$ -wave up to 10 mK, when the  $p$ -wave takes over. The atom exchange rate, already discussed, has a major contribution from the  $p$ -wave, which raises above the  $s$ -wave around 0.1 mK, while the  $d$ -wave up to 0.1 K is not relevant.

The dissociation component of the loss rate has an overwhelming contribution from the  $p$ -wave up to about 10 mK, when the  $d$ -wave becomes competitive due to its contribution, essentially, to the dissociation process. We have to remind that the  $p$ - and  $d$ -waves are determined by the bindings energies of the diatomic molecules  ${}^4\text{He}_2$  and the very weakly bound  ${}^4\text{He}^6\text{Li}$ , which gives a long range tail for the attractive Efimov like potential [42], that of course damps the centrifugal barrier enhancing the importance of the higher partial waves, even at low energies. The relative relevance of the  $d$ -wave contribution can be clearly seen in the loss rate.

Comparing the calculations of the zero- and finite-range potential models, for the same inputs from the set (a1), it is clear the independence of the bulk results on the detail of the potential beyond the dimer and trimer binding energies. Both models exhibit a strong enhancement of the atom exchange and loss rates between 2-3 mK, increasing up to  $10^{-9}\text{cm}^3/\text{s}$ , with the  $p$ -wave playing a major role.

For the model (a2), the  ${}^6\text{Li} + {}^4\text{He}_2 \rightarrow {}^4\text{He} + {}^4\text{He}^6\text{Li}$  reaction is endothermic, as seen from the Table III. The corresponding results are given in Fig. 6, where the atom exchange channel opens at 1.2mK and the dissociation at 1.3mK, offering an interesting interplay between the competing losses in these two channels. For the elastic reaction rate, the  $s$ -wave contribution is relevant below 1mK, with the  $p$ -wave being dominant above 10mK, while the  $d$ -wave is marginal. In the atom exchange rate the  $s$ - and  $d$ -waves are present, although the  $p$ -wave contributes to a large extend.

The loss rate corresponds essentially to the atom exchange rate up to 5mK, while above 10mK it receives contribution from the dissociation process in both  $p$ - and  $d$ -waves, which attains values on the bold part of  $10^{-9}\text{cm}^3/\text{s}$ . The relevant contributions from the  $p$ - and  $d$ -waves amounts to the smallest of the binding energy of the  ${}^4\text{He}^6\text{Li}$  molecule, which extends the Efimov long range potential, increasing the relevance of  $p$ - and  $d$ -waves to the reaction process.



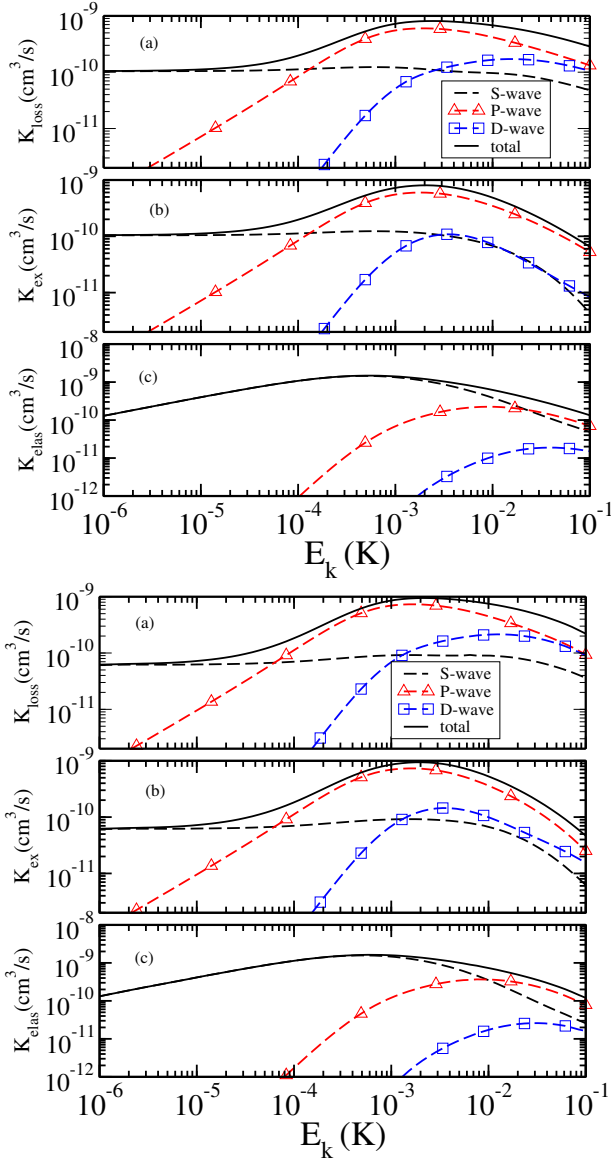


FIG. 5. Reaction rates for  ${}^6\text{Li} + {}^4\text{He}_2$ , using zero-range (upper-set of panels) and finite-range (lower-set of panels) interactions, considering the (a1) model.

## V. THREE BODY REACTIONS WITH HELIUM-4 AND LITHIUM-7

### A. Reaction rates for ${}^4\text{He} + {}^4\text{He}{}^7\text{Li}$

In this section, we report our results on the elastic, exchange and loss rates for the system containing the  ${}^7\text{Li}$  isotope, namely, when considering the  ${}^4\text{He} + {}^4\text{He}{}^7\text{Li}$  reaction, which has the diatomic and triatomic molecules more bound than the previous case where the Lithium-6 isotope was interacting with the other two  ${}^4\text{He}$  atoms. For the inputs of the zero and finite-range models, the corresponding parameters for the potentials (a1) and (a2) are given in Table I. For both sets (a1) and (a2) the reaction  ${}^4\text{He} + {}^4\text{He}{}^7\text{Li} \rightarrow {}^4\text{He}_2 + {}^7\text{Li}$  is endothermic, with the corresponding binding energies being quite close. As verified, the results for the rates are very much

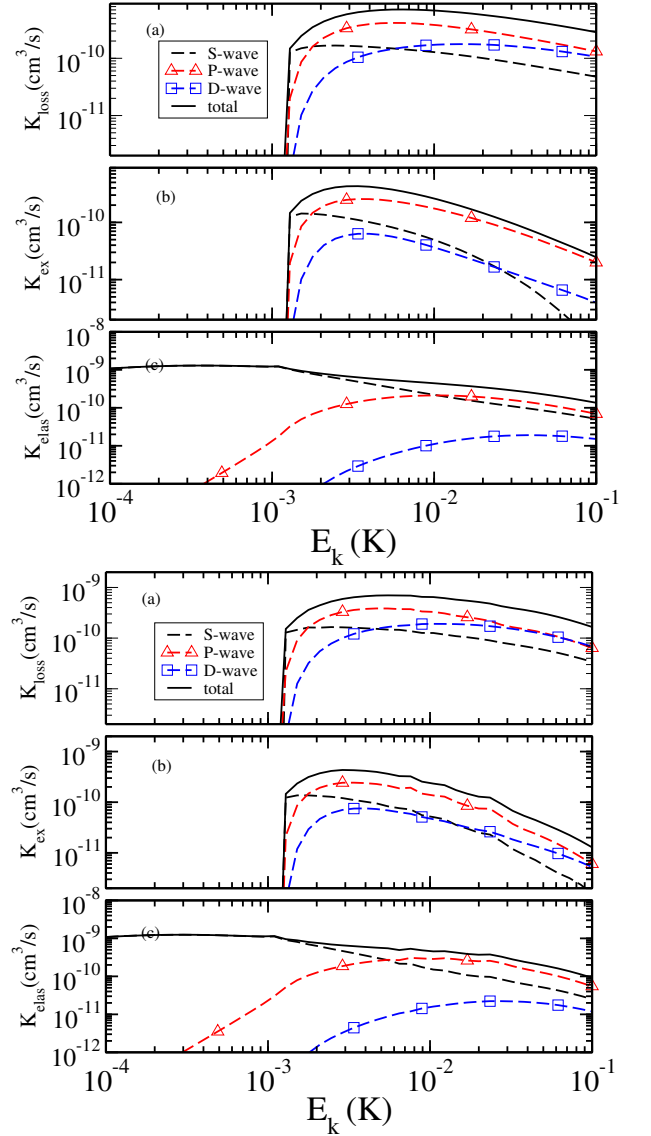


FIG. 6. Reaction rates for  ${}^6\text{Li} + {}^4\text{He}_2$ , using zero-range (upper-set of panels) and finite-range (lower-set of panels) interactions, considering the (a2) model.

similar, as it will be detailed in our discussion of Figs. 7 and 8. In this case, the separable potential has the scattering lengths much larger than the effective range, namely, about one order of magnitude and above, as seen in Table II, making the outcome of the zero-range model closer to the results obtained with the finite range potential, as the corrections due to the effective range are marginal.

In Fig. 7, the reaction rates for the parameter set (a1) are shown, where the atom exchange channel opens around 4.3mK, and close to this energy the  $p$ -wave elastic phase shift has a zero, clearly seen for the zero-range and finite range models. The  $s$ -wave amplitude gives the elastic rate up to the atom exchange threshold, when the  $p$ -wave becomes dominant, this is noticed by a depression in the rate, independent of the model. The atom exchange rate is essentially defined by the  $p$ -wave, as we have discussed before. The loss rate in the  $d$ -wave becomes relevant at energies of about 100 mK.

The calculations of the reaction rates with the parameter

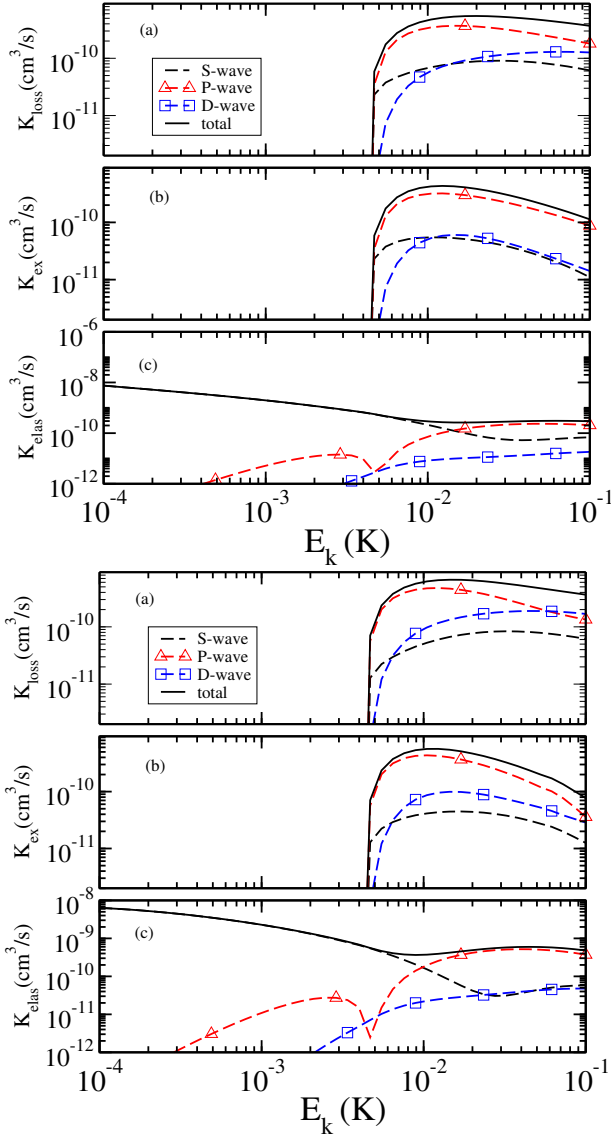


FIG. 7. Reaction rates for  ${}^4\text{He} + {}^4\text{He}^7\text{Li}$ , using zero-range (upper-set of panels) and finite-range (lower-set of panels) interactions, considering the (a1) model.

set (a2) are shown in Fig. 8 for the  ${}^4\text{He} + {}^4\text{He}^7\text{Li}$  collision. In this case the atom exchange reaction opens close to 1mK. Interesting enough is the zero of the elastic  $p$ -wave phase shift close to the threshold, as seen by the minimum of the elastic rate close to the atom exchange threshold. This minimum seems a universal property of the  $p$ -wave also appearing in the elastic process with model (a1). The difference between the two parameter sets is the binding energy of the  ${}^4\text{He}^7\text{Li}$  molecule, as the triatomic binding energy is not relevant for the  $p$ -wave, which is also the protagonist on both the atom exchange and loss rate. The  $s$ -wave has a minor contribution on these two rates, and the  $d$ -wave appears in the loss rate above 100mK. The bulk of the results for the reaction rates are unaffected by the change of the potential range.

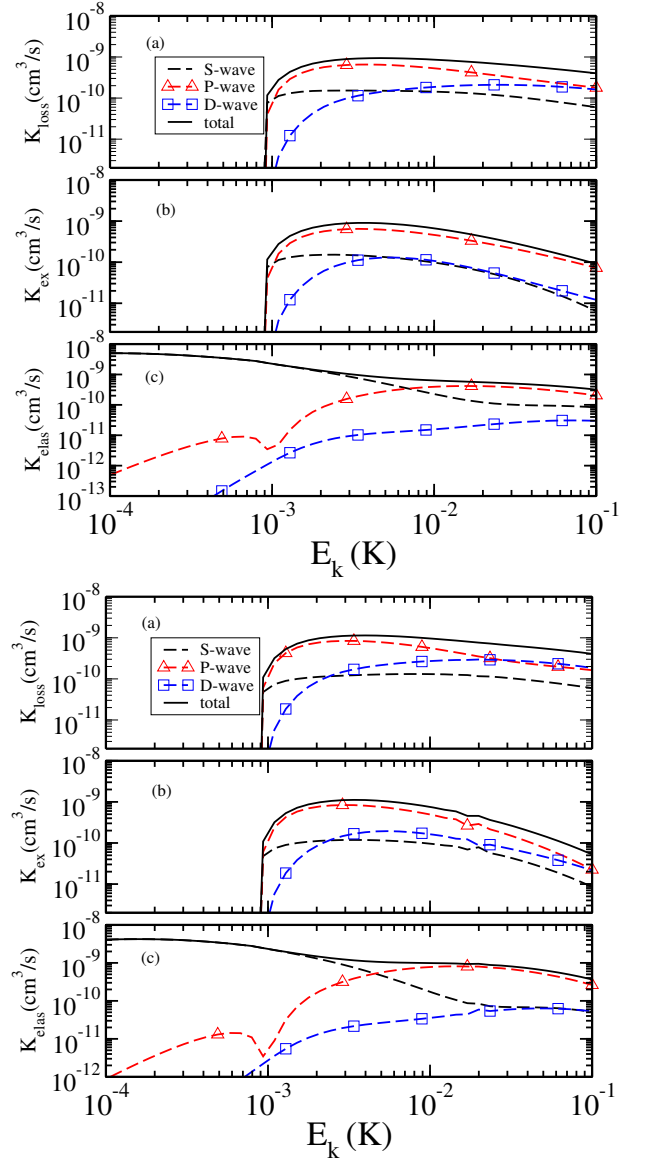


FIG. 8. Reaction rates for  ${}^4\text{He} + ({}^4\text{He}^7\text{Li})$ , using zero-range (upper-set of panels) and finite-range (lower-set of panels) interactions, considering the (a2) model.

### B. Reaction rates for ${}^7\text{Li} + {}^4\text{He}_2$

Our results on the reaction rates for  ${}^7\text{Li} + {}^4\text{He}_2$ , presented in the Figs. 9 and 10, are discussed in this subsection. As represented in Table II, the atom exchange channel is exothermic for both set of potential models (a1) and (a2), with the dissociation threshold appearing at 1.3mK for both two cases.

The results for the zero and finite-range models with parameters obtained from (a1), given in Table I, are shown in Fig. 9. The  $s$ -wave dominates the elastic rate up to the dissociation threshold, when the  $p$ -wave takes over and gives the total value for the rate. The exothermic atom exchange reaction, i.e.,  ${}^7\text{Li} + {}^4\text{He}_2 \rightarrow {}^4\text{He} + {}^4\text{He}^7\text{Li}$ , has the major contribution from the  $s$ -wave up to about 0.1mK, when the  $p$ -wave dominates. The loss rate shows the relevance of the  $p$ -wave up to 100mK, when the  $d$ -wave starts to compete. Both zero-range and separable potential models provide very similar model independent results. So, for the results obtained in

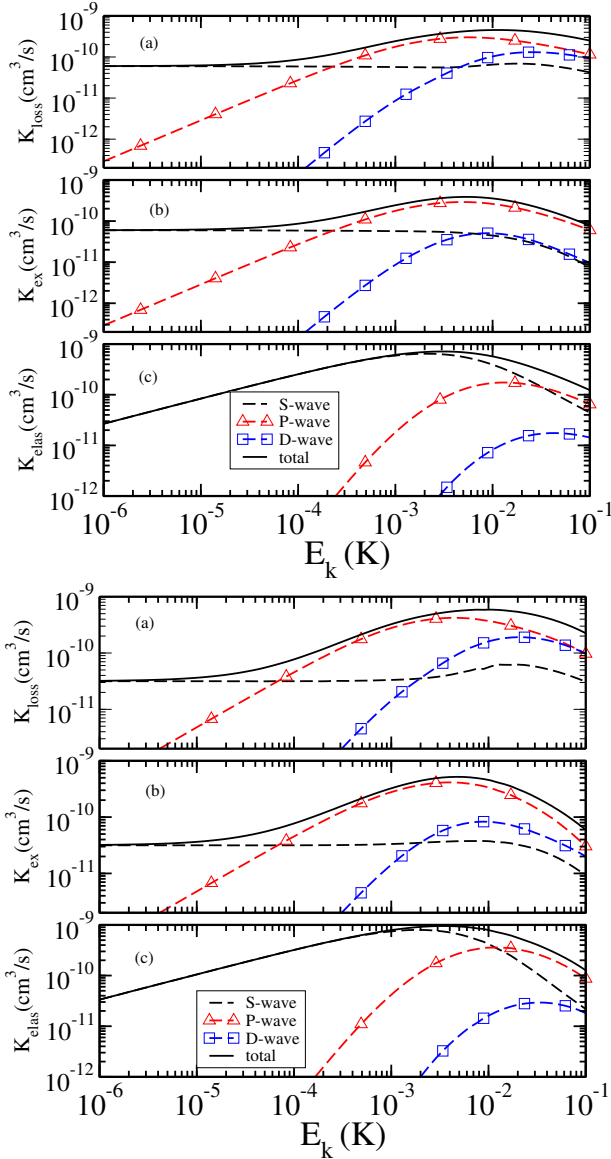


FIG. 9. Reaction rates for  ${}^7\text{Li} + {}^4\text{He}_2$ , using zero-range (upper-set of panels) and finite-range (lower-set of panels) interactions, considering the (a1) model.

these calculations, it seems not relevant the interaction range.

The next set of calculations were performed for the zero and finite-range models with the parameters (a2), given in Table I, and presented in Fig. 10. Comparing with the binding energies from the set (a1), the corresponding values for the diatomic and triatomic molecules are more weakly bound, of about half of the corresponding values. This is reflected in the  $s$ -wave elastic rates that are about three times larger below 0.1mK, while the maximum is about the same and somewhat below 10mK, with value of  $10^{-9}\text{cm}^3/\text{s}$ . This is a consequence of the large difference in the binding energies of  ${}^4\text{He}_2$ - ${}^7\text{Li}$  molecule, which for set (a2) is considerably smaller than set (a1). The  $p$ -wave outcome is only sensitive to the diatomic binding energies, with  ${}^4\text{He}_2$  and  ${}^4\text{He}{}^7\text{Li}$  changing from 5.6 to 2.16 mK, that explains the results being quite close, as well as for the  $d$ -wave.

The exothermic atom exchange reaction rate shown in Fig. 10 has the dominance of the  $s$ -wave up to about 0.1mK,

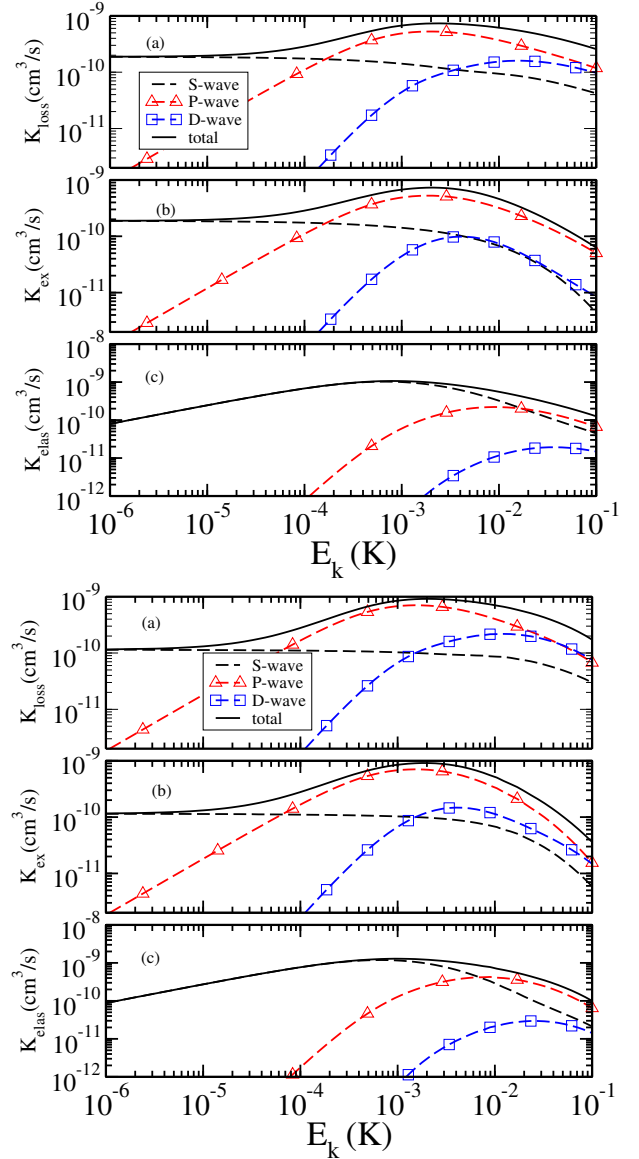


FIG. 10. Reaction rates for  ${}^7\text{Li} + {}^4\text{He}_2$ , using zero-range (upper-set of panels) and finite-range (lower-set of panels) interactions, considering the (a2) model.

when the  $p$ -wave rises and gives the bulk part of the rate. The  $p$ -wave also dominates the loss rate up to 10mK, when the  $d$ -wave starts to compete. The comparison between the zero-range and separable potential model results shows again the model independence, with the finite range playing a minor role to build the bulk values of the calculated rates.

## VI. THREE BODY REACTIONS WITH HELIUM AND SODIUM

### A. Reactions rates for ${}^4\text{He} + {}^4\text{He}{}^{23}\text{Na}$

The collision  ${}^4\text{He} + {}^4\text{He}{}^{23}\text{Na}$  process has some distinctive features compared to the previous cases composed by helium and lithium atoms. Two salient differences will be apparent in the rate results. For this case, the parametrization of the sep-

arable potential gives an effective range, which is only about half of the scattering length, as shown in Table II. The other feature is the presence of Efimov zeros in the elastic  $s$ -wave phase-shift [43].

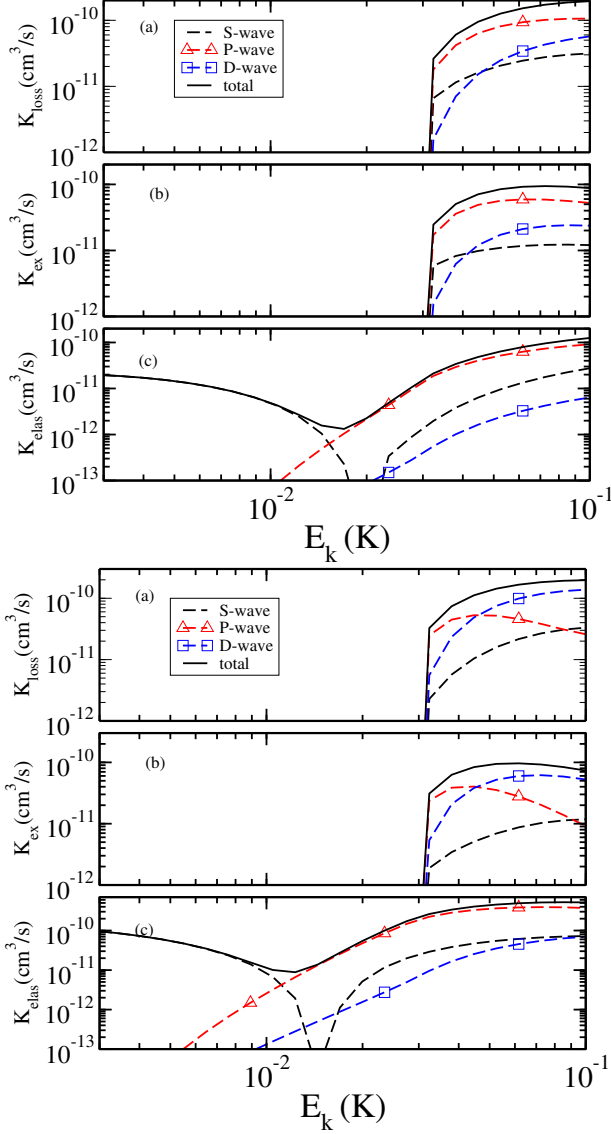


FIG. 11. Reaction rates for  ${}^4\text{He} + {}^4\text{He}^{23}\text{Na}$ , using zero-range (upper-set of panels) and finite-range (lower-set of panels) interactions, considering the (a1) model.

The Efimov zeros are a sequence of zeros/dips in the elastic scattering amplitude, that are controlled by both the scattering lengths and the actual value of the triatomic binding energy [43]. The  ${}^4\text{He} + {}^4\text{He}^{23}\text{Na}$   $s$ -wave phase-shift presents such a zero/dip, which is sensitive both to the two-atom low energy parameters and to the short range physics summarized in the binding energy of  ${}^4\text{He}_2-{}^{23}\text{Na}$  molecule. The zero turns into a dip, if it appears above the threshold of the atom-exchange or dissociation channels, due to the probability flux from the elastic channel to those ones.

The atom-exchange reaction is now endothermic for  ${}^4\text{He} + {}^4\text{He}^{23}\text{Na} \rightarrow {}^4\text{He}_2 + {}^{23}\text{Na}$  and this channel opens around 28mK, while the dissociation reactions happens above 29mK, for both parameter sets (a1) and (a2) (see Table III). Our results for the reaction rates obtained with the zero-range

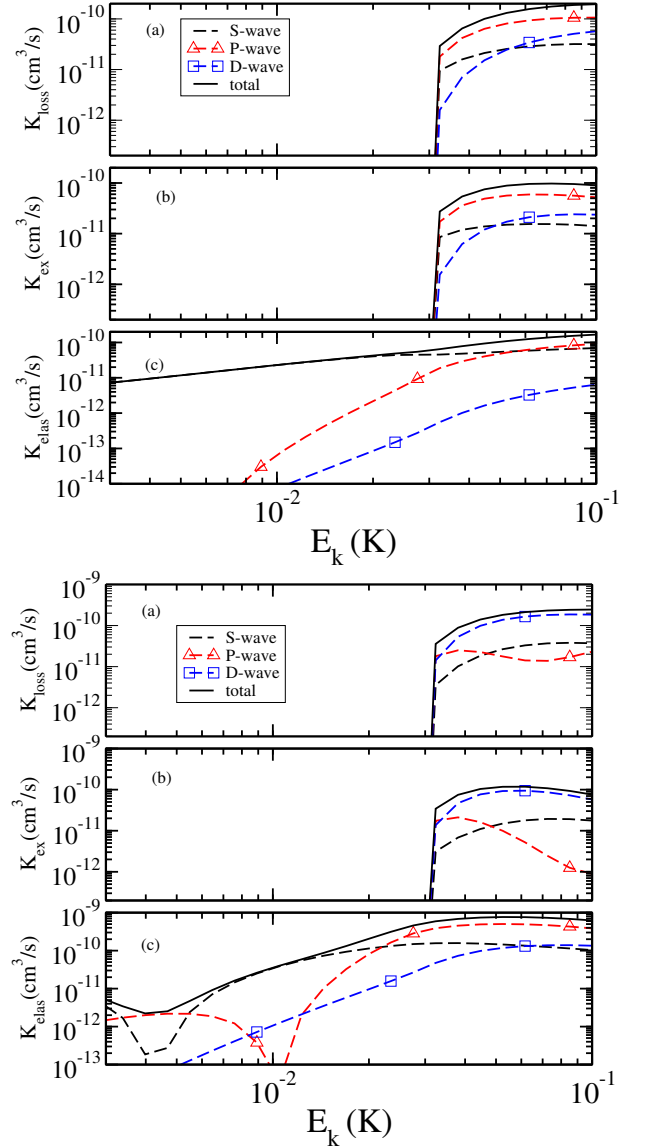


FIG. 12. Reaction rates for  ${}^4\text{He} + {}^4\text{He}^{23}\text{Na}$ , using zero-range (upper-set of panels) and finite-range (lower-set of panels) interactions, considering the (a2) model.

and separable potential models with parameter sets (a1) and (a2) are shown in Figs. 11 and 12, respectively.

In Figs. 11 and 12, the calculations of the reaction rates for the helium collision with ( ${}^4\text{He}^{23}\text{Na}$ ) molecule are shown for both zero and finite range separable potentials. It is interesting to observe that the Efimov zero of the elastic  $s$ -wave phase-shift and corresponding reaction rate appears for the zero-range and one-term Yamaguchi separable potentials respectively at 20mK and 15mK for the set (a1). In the case of the parameter set (a2), the zero of the elastic rate for the potential comes around 2.5mK, while for the zero-range model the zero is not present in the scale of the figure. The effective range moves the zero to somewhat larger values of the energy. These zeros are quite sensitive to the difference in the on-shell parameters as one can appreciate in Tables I and II.

The two potential models have identical diatomic and  ${}^4\text{He}_2-{}^{23}\text{Na}$  binding energies for the parameter set (a1), but they differ in the effective range and scattering lengths, which

combined produce the change in the position of the  $s$ -wave zero, while keeping the same qualitative features in the elastic rate. The zero of the  $s$ -wave elastic reaction rate gives together with the dominant  $p$ -wave contribution a pronounced dip, which for (a1) comes around 12-15mK, and the elastic rate from this energy up to 50 mK, increases two orders of magnitude to about  $10^{-9}\text{cm}^3/\text{s}$ . The same qualitative feature is found for the parameter set (a2), with the dip around 2.5mK for the separable potential, while for the zero-range model it is not present in the scale of the figure. The position of the minimum is sensitive to the effective range, as already observed for the parameter set (a1). For both parameter sets (a1) and (a2) the  $p$ -wave turns to be relevant between 10 and 30mK, while for the one-term separable potential with set (a2) it presents a zero.

The atom exchange and loss rates are dominated by the higher waves, with particular preponderance of the  $p$ -wave, as found for the triatomic systems with the lithium isotopes. When considering the sets (a1) and (a2) parametrized by Yamaguchi potentials, the influence of the effective range is verified in both cases by the importance of the  $d$ -wave with respect to the  $p$ -wave contribution. Naively, one can understand the effect of the effective range on the imbalance of the  $p$ - and  $d$ -waves, as it cuts the long-range Efimov potential, which is relatively more important for the  $p$ -wave than for the  $d$ -wave. In the zero range model, without the weakening of the long range potential, the  $p$ -wave is dominant on the exchange and loss rates.

### B. Reaction rates for $^{23}\text{Na} + ^4\text{He}_2$

The reaction  $^{23}\text{Na} + ^4\text{He}_2$  has an exothermic channel with the atom exchange to form the  $^4\text{He}_2\text{-}^{23}\text{Na}$  molecule (see Table III), and the dissociation threshold is quite low at 1.31mK, for both set of parameters (a1) and (a2). The results are shown in Figs. 13 and 14, for both zero-range and one-term separable Yamaguchi potentials with parameter sets (a1) and (a2), respectively. The magnitude of the reaction rates are found to grow up to  $10^{-10}\text{cm}^3/\text{s}$ . These values are one order below the reaction rates obtained with the isotopes of lithium with mass numbers 6 and 7, as we have thoroughly discussed in sections IV B and V B.

The elastic reaction rate is dominated by the  $s$ -wave up to about 10mK, independent of the parameter set (a1) or (a2) and potential range, as shown in Figs. 13 and 14. The  $p$ -wave importance above such energies increases over the  $s$ - and  $d$ -waves. The atom exchange process is open for this entrance reaction channel, and the  $p$ -wave contributes to the bulk of this rate above 1mK, while the  $d$ -wave becomes more relevant with respect to the  $p$ -wave for the finite range potential. This happens due to the fact that the finite range of the potential has the effect to deplete the  $p$ -wave rate, as we have discussed before. This behavior is independent of the parameter set (a1) or (a2).

Finally the dissociation rate component of  $K_{\text{loss}}$  is essentially determined by the  $p$ - and  $d$ -waves, with the  $s$ -wave contributing marginally. The inversion of the importance of the  $p$ - and  $d$ -waves to the dissociation process comes as a consequence of the consideration of the effective range. By analyzing separately the elastic and loss rates, one can disentangle the two and three-atomic low energy input informations contained  $s$ -,  $p$ - and  $d$ -waves. Specifically, the  $s$ -wave re-

action rates depends on two and three-atomic low energy input informations, while the higher partial waves mainly carry the diatomic low energy parameters and being insensible to the triatomic molecular energy. By taking into account experimental differential angular reaction rates the individual partial waves could be extracted. Following this procedure, real possibilities exist to separate the effects of the triatomic molecule binding energy from the diatomic low energy informations, namely, binding energy, scattering length and effective range, which are contained in the elastic atom exchange and total loss rate from eventual experimental data below 100mK.

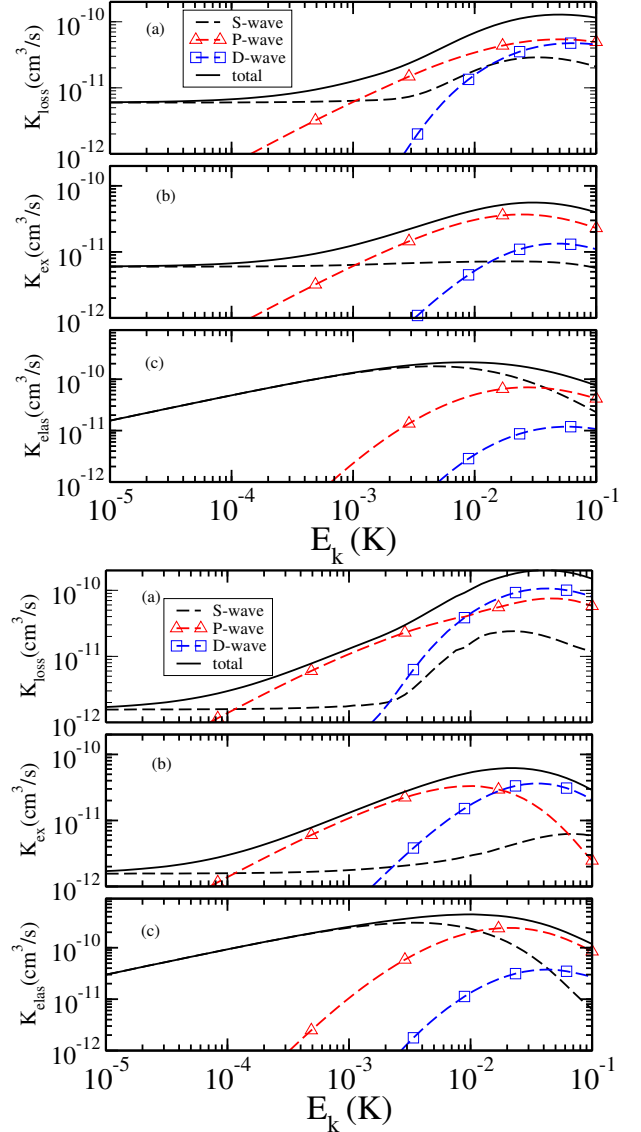


FIG. 13. Reaction rates for  $^{23}\text{Na} + ^4\text{He}_2$ , using zero-range (upper-set of panels) and finite-range (lower-set of panels) interactions, considering the (a1) model.

## VII. CONCLUSION

In the present work, we provide predictions for several atom-dimer reaction rates, by considering particular two-atomic systems for different configurations having two  $^4\text{He}$



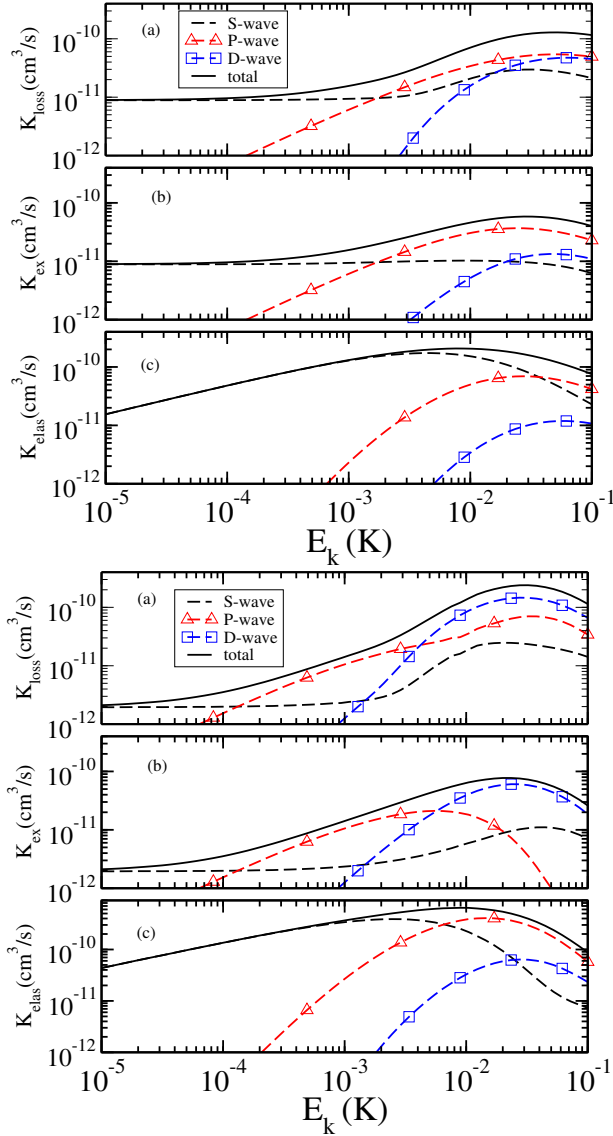


FIG. 14. Reaction rates for  $^{23}\text{Na} + {}^4\text{He}_2$ , using zero-range (upper-set of panels) and finite-range (lower-set of panels) interactions, considering the (a2) model.

atoms with one of the species, among  ${}^6\text{Li}$ ,  ${}^7\text{Li}$  and  ${}^{23}\text{Na}$ , taking the advantage that dimer and trimer binding energies are available for these atom-dimer systems from experimental data or predicted by realistic potential model calculations. Within the Faddeev formalism approach, these realistic binding energies are directly applied, in our study with zero-range and finite-range two-body interactions. We predict reaction rates for cold  ${}^4\text{He}$  elastic collisions with  ${}^4\text{He}{}^6\text{Li}$ ,  ${}^4\text{He}{}^7\text{Li}$  and  ${}^4\text{He}{}^{23}\text{Na}$  molecules, as well as by considering the atomic species  ${}^6\text{Li}$ ,  ${}^7\text{Li}$  and  ${}^{23}\text{Na}$  reacting with helium dimers for center-of-mass kinetic energies up to 100 mK.

For our study we use the diatomic and triatomic parameters from two atomic models given in [86]. The elastic, atom exchange and loss rates are computed with a zero-range and a  $s$ -wave one-term separable potential in order to access the relevance of the effective range, besides the diatomic binding energies from [86]. This work follows a previous exploration of the cold  $s$ -wave cross-sections for the  ${}^4\text{He}$  on the diatomic molecules formed by the helium atom with the isotopes of

lithium and sodium [43] using the zero-range and one-term separable potentials.

Specifically, the elastic, atom-exchange and dissociation channels are investigated for the following six reactions:

- ${}^4\text{He} + {}^4\text{He}{}^6\text{Li}$  and  ${}^6\text{Li} + {}^4\text{He}_2$ , in Section IV;
- ${}^4\text{He} + {}^4\text{He}{}^7\text{Li}$  and  ${}^7\text{Li} + {}^4\text{He}_2$ , in Section V;
- ${}^4\text{He} + {}^4\text{He}{}^{23}\text{Na}$  and  ${}^{23}\text{Na} + {}^4\text{He}_2$ , in Section VI.

The main characteristic found in these studies is the  $p$ -wave dominance of the atom-exchange and dissociation reaction, allowing the separation of the effects of the on-shell low energy diatomic properties from the triatomic binding energy, which is determinant for the elastic reaction rate below the dissociation threshold. In particular, for the  ${}^6,{}^7\text{Li}$  and  ${}^{23}\text{Na}$  reactions with the  ${}^4\text{He}_2$  dimer, the atom exchange channel is always open, which allows to separate the  $s$ -wave contribution below the dissociation threshold from the higher partial wave rates.

Of possible experimental relevance, is the presence of a minimum in the  $s$ -wave elastic reaction rate for the  ${}^4\text{He} \rightarrow ({}^4\text{He}{}^{23}\text{Na})$  scattering, following the previous findings of Ref. [43]. This minimum is kept once the other partial waves are included in the elastic rate, and thus could be of interest from the point of view of an actual experiment. Such minimum is reminiscent of the Efimov effect that translates in the scattering region as a log periodicity of zeros in the elastic  $s$ -wave phase shift in the collision of the atom with a weakly bound dimer. Another interesting property is the presence of a zero/dip for some of the elastic rate in the  $p$ -wave, which was particularly seen in the case of  ${}^4\text{He} + ({}^4\text{He}{}^7\text{Li})$  and  ${}^4\text{He} + ({}^4\text{He}{}^{23}\text{Na})$  between 1 and 10mK.

The atom exchange and dissociation rates for all examples we have studied is dominated by the  $p$ -wave, as it is understood from the importance of the one atom exchange mechanism, which gives more weight to the process at backward angles. Pictorially, one of the atoms in the initial molecule is picked-up by the incoming atom, and the newly formed molecule is propagating backwards. We remind that already the kernel of the integral equations and inhomogeneous term for the zero-range and  $s$ -wave one term separable potential corresponds to an atom exchange amplitude.

The range correction to the reaction rates computed with the one-term separable potential, is particularly noticeable as an inversion of the relative importance between the  $p$ - and  $d$ -waves, with respect to the results obtained with the zero-range model. This effect comes from the softening of the long-range Efimov type potential at the short distances due to the finite range, still perceptible for the  $p$ -wave, while the  $d$ -wave is less sensitive to such modification due to the stronger centrifugal barrier. Therefore, such an effect emphasizes even more the possibility to disentangle the on-shell low energy two-atom informations and the triatomic binding energy, with the last one is determinant for the  $s$ -wave rates, but irrelevant for the higher wave contributions. The  $p$ - and  $d$ -wave dominate the atom exchange and dissociation rates, while presenting different sensitivities to the low energy diatomic parameters.

Although the results for the reaction rates present some sensitivity to the potential range when the fitted potential presents effective ranges comparable to the scattering length, which is found particularly for the  ${}^4\text{He}{}^4\text{He}{}^{23}\text{Na}$ , still the bulk values obtained with the zero range and the finite range potential are similar, supporting the robustness of our predictions.



Closing our summary, we should point to some future directions of our investigation. The methods employed here can be extended to ultracold atoms in atomic traps to study controlled chemical reactions, by means of tuning the scattering lengths with Feshbach resonances, and also moving the triatomic state by induced few-body forces [96]. In addition, more complex reactions considering the collision of diatomic molecules widens the scope of our investigation. Another perspective is the manipulation of the aspect ratio of the trap, changing the effective dimension in which the reaction takes place in a continuous way from three to two dimensions [97–100], therefore we hope that in the future not only the interaction can be tuned but also the effective dimension. **Acknowledgments** This work was partially supported by Fundação de Amparo à Pesquisa do Estado de São Paulo [2017/05660-0 (TF and LT), 2019/00153-8 (MTY)], Coordenação de Aperfeiçoamento de Pessoal de Nível Superior (MAS), Conselho Nacional de Desenvolvimento Científico e Tecnológico [303579/2019-6 (MTY), 308486/2015-3 (TF), 304469-2019-0 (LT), and Project INCT-FNA 464898/2014-5].

## Appendix A: Atom-dimer transition operators

As considering the particles  $i$  and  $j$  ( $= 1, 2, 3$ ), the general three-body scattering formalism, when the particle  $i$  is the projectile, can be written in operator form as [87, 88]

$$U_{ji} = \bar{\delta}_{ji} G_0^{-1} + \sum_k \bar{\delta}_{kj} t_k G_0 U_{ki} \quad (\text{A1})$$

where  $U_{ji}$ s are transition amplitudes,  $t_k$ s are two body T-matrices and  $G_0$  is three-body free propagator. If particle 1 is the projectile  $U_{11}$  is related to elastic scattering amplitude and  $U_{21}$  and  $U_{31}$  are related to rearrangement amplitudes. By multiplying the both sides of Eq. (A1) from right and left to  $G_0$ :

$$\begin{aligned} G_0 U_{11} G_0 &= G_0 t_2 G_0 U_{21} G_0 + G_0 t_3 G_0 U_{31} G_0 \\ G_0 U_{21} G_0 &= G_0 + G_0 t_1 G_0 U_{11} G_0 + G_0 t_3 G_0 U_{31} G_0 \\ G_0 U_{31} G_0 &= G_0 + G_0 t_1 G_0 U_{11} G_0 + G_0 t_2 G_0 U_{21} G_0 \end{aligned} \quad (\text{A2})$$

If we use separable potential for two-body interactions, we will have the following two-body T-matrices.

$$\begin{aligned} t_i &= |g_i\rangle \tau_i \langle g_i| \\ \langle \mathbf{p} \mathbf{q} | t_i | \mathbf{p}' \mathbf{q}' \rangle &= \delta(\mathbf{p} - \mathbf{p}') \delta(\mathbf{q} - \mathbf{q}') \tau(E_3 - \frac{q^2}{2\mu_{iq}}), \end{aligned} \quad (\text{A3})$$

where  $|g_i\rangle$  is called the form factor. By introducing the following operators:

$$\begin{aligned} X_{ij} &= \langle g_i | G_0 U_{ij} G_0 | g_j \rangle, \\ Y_{ij} &= \langle g_i | G_0 | g_j \rangle \end{aligned} \quad (\text{A4})$$

we will have:

$$\begin{aligned} X_{11} &= Y_{12} \tau_2 X_{21} + Y_{13} \tau_3 X_{31}, \\ X_{21} &= Y_{21} + Y_{21} \tau_1 X_{11} + Y_{23} \tau_3 X_{31}, \\ X_{31} &= Y_{31} + Y_{31} \tau_1 X_{11} + Y_{32} \tau_2 X_{21}. \end{aligned} \quad (\text{A5})$$

We consider  $X_{ij}(\mathbf{q}, \mathbf{q}') = \langle \mathbf{q} | X_{ij} | \mathbf{q}' \rangle$  and  $Y_{ij}(\mathbf{q}, \mathbf{q}') = \langle \mathbf{q} | Y_{ij} | \mathbf{q}' \rangle$ . For the scattering of a particle  $\alpha$  by the  $\alpha\beta$  bound subsystem, we have  $1 \rightarrow \alpha$ ,  $2 \rightarrow \alpha$  and  $3 \rightarrow \beta$ . Using symmetry property for the identical bosons, we consider

$X_{11}(\mathbf{q}, \mathbf{q}') + X_{21}(\mathbf{q}, \mathbf{q}') = X(\mathbf{q}, \mathbf{q}')$  for elastic scattering and  $X_{31}(\mathbf{q}, \mathbf{q}') = X'(\mathbf{q}, \mathbf{q}')$  for rearrangement. We can also calculate:

$$\begin{aligned} Y_{13}(\mathbf{q}, \mathbf{q}') &= Y_{31}(\mathbf{q}', \mathbf{q}) = Y_{23}(\mathbf{q}, \mathbf{q}') = Y_{32}(\mathbf{q}', \mathbf{q}) = \frac{K_1(\mathbf{q}, \mathbf{q}')}{2}, \\ Y_{12}(\mathbf{q}, \mathbf{q}') &= Y_{12}(\mathbf{q}', \mathbf{q}) = Y_{21}(\mathbf{q}, \mathbf{q}') = Y_{21}(\mathbf{q}', \mathbf{q}) = \frac{K_2(\mathbf{q}, \mathbf{q}')}{2}, \end{aligned} \quad (\text{A6})$$

and we can write the partial wave decomposition of the coupled equations (A5), as follows:

$$\begin{aligned} X^\ell(q, q') &= \frac{K_2^\ell(q, q')}{2} \\ &+ 4\pi \int k^2 dk \frac{K_2^\ell(q, k)}{2} \tau_{\alpha\beta}(k; E_3) X^\ell(k, q') \\ &+ 4\pi \int k^2 dk K_1^\ell(q, k) \tau_{\alpha\alpha}(k; E_3) X'^\ell(k, q'), \\ X'^\ell(q, q') &= \frac{K_1^\ell(q', q)}{2} \\ &+ 4\pi \int k^2 dk \frac{K_1^\ell(k, q)}{2} \tau_{\alpha\alpha}(k; E_3) X^\ell(k, q'), \end{aligned} \quad (\text{A7})$$

where  $\tau_1(E_3 - \frac{k^2}{2\mu_{\alpha(\alpha\beta)}}) = \tau_2(E_3 - \frac{k^2}{2\mu_{\alpha(\alpha\beta)}}) = \tau_{\alpha\beta}(k; E_3)$  and  $\tau_3(E_3 - \frac{k^2}{2\mu_{\beta(\alpha\alpha)}}) = \tau_{\alpha\alpha}(k; E_3)$ . By removing the singularity of two-body T-matrices:

$$\begin{aligned} \tau_{\alpha\beta}(q; E_3) &= \frac{\bar{\tau}_{\alpha\beta}(q; E_3)}{q^2 - k_\alpha^2 - i\epsilon}, \\ \tau_{\alpha\alpha}(q; E_3) &= \frac{\bar{\tau}_{\alpha\alpha}(q; E_3)}{q^2 - k_\beta^2 - i\epsilon}. \end{aligned} \quad (\text{A8})$$

We introduce the scattering and rearrangement reduced amplitudes as follow:

$$\begin{aligned} h_\alpha^\ell(q, q') &= 2\pi^2 \bar{\tau}_{\alpha\beta}(q; E_3) X^\ell(q, q'), \\ h_\beta^\ell(q, q') &= 4\pi^2 \bar{\tau}_{\alpha\alpha}(q; E_3) X'^\ell(q, q'), \end{aligned} \quad (\text{A9})$$

and using Eq. (A9) in Eq. (A7) we find the following equations for the half-on-shell scattering and rearrangement reduced amplitudes:

$$\begin{aligned} h_\alpha^\ell(q; E_3) &= \bar{\tau}_\alpha(q; E_3) \left\{ \frac{\pi}{2} K_2^\ell(q, k_\alpha; E_3) + \int_0^\infty dk k^2 \times \right. \\ &\times \left[ K_2^\ell(q, k; E_3) \frac{h_\alpha^\ell(k; E_3)}{(k^2 - k_\alpha^2 - i\epsilon)} + K_1^\ell(q, k; E_3) \frac{h_\beta^\ell(k; E_3)}{q^2 - k_\beta^2 - i\epsilon} \right] \Big\}, \\ h_\beta^\ell(q; E_3) &= \bar{\tau}_\beta(q; E_3) \left\{ \frac{\pi}{2} K_1^\ell(k_\alpha, q; E_3) \right. \\ &+ \left. \int_0^\infty dk k^2 K_1^\ell(k, q; E_3) \frac{h_\alpha^\ell(k; E_3)}{(k^2 - k_\alpha^2 - i\epsilon)} \right\}, \end{aligned} \quad (\text{A10})$$

where  $q' = k_\alpha = \sqrt{2\mu_{\alpha(\alpha\beta)}(E_3 - E_{\alpha\beta})}$  and

$$\begin{aligned} \bar{\tau}_\alpha(q; E_3) &= 2\pi \bar{\tau}_{\alpha\beta}(q; E_3), \\ \bar{\tau}_\beta(q; E_3) &= 4\pi \bar{\tau}_{\alpha\alpha}(q; E_3). \end{aligned} \quad (\text{A11})$$

For the scattering of a particle  $\beta$  by the  $\alpha\alpha$  bound subsystem, we have  $1 \rightarrow \beta$ ,  $2 \rightarrow \alpha$  and  $3 \rightarrow \alpha$ . Using symmetry property for the identical bosons, we consider

$X'(\mathbf{q}, \mathbf{q}') \equiv X_{11}(\mathbf{q}, \mathbf{q}')$  for elastic scattering and  $X(\mathbf{q}, \mathbf{q}') \equiv X_{21}(\mathbf{q}, \mathbf{q}') + X_{31}(\mathbf{q}, \mathbf{q}')$  for rearrangement. We can also calculate:

$$\begin{aligned} Y_{12}(\mathbf{q}, \mathbf{q}') &= Y_{21}(\mathbf{q}', \mathbf{q}) = Y_{13}(\mathbf{q}, \mathbf{q}') = Y_{31}(\mathbf{q}', \mathbf{q}) = \frac{K_1(\mathbf{q}', \mathbf{q})}{2}, \\ Y_{23}(\mathbf{q}, \mathbf{q}') &= Y_{23}(\mathbf{q}', \mathbf{q}) = Y_{32}(\mathbf{q}, \mathbf{q}') = Y_{32}(\mathbf{q}', \mathbf{q}) = \frac{K_2(\mathbf{q}, \mathbf{q}')}{2}, \end{aligned} \quad (\text{A12})$$

and we can write Eq. (A5) as follows:

$$\begin{aligned} X^\ell(q, q') &= K_1^\ell(q, q') \\ &+ 4\pi \int k^2 dk \frac{K_2^\ell(q, k)}{2} \tau_{\alpha\beta}(k; E_3) X^\ell(k, q') \\ &+ 4\pi \int k^2 dk K_1^\ell(q, k) \tau_{\alpha\alpha}(k; E_3) X'^\ell(k, q') \\ X'^\ell(q, q') &= 4\pi \int k^2 dk \frac{K_1^\ell(k, q)}{2} \tau_{\alpha\alpha}(k; E_3) X^\ell(k, q') \end{aligned} \quad (\text{A13})$$

Using Eq. (A9) in (A13) we have the following equations for the half-on-shell scattering and rearrangement reduced amplitudes:

$$\begin{aligned} h_\alpha^\ell(q; E_3) &= \bar{\tau}_\alpha(q; E_3) \left\{ \pi K_1^\ell(q, k_\alpha; E_3) + \int_0^\infty dk k^2 \times \right. \\ &\times \left[ K_2^\ell(q, k; E_3) \frac{h_\alpha^\ell(k; E_3)}{(k^2 - k_\alpha^2 - i\epsilon)} + K_1^\ell(q, k; E_3) \frac{h_\beta^\ell(k; E_3)}{q^2 - k_\beta^2 - i\epsilon} \right] \Big\}, \\ h_\beta^\ell(q; E_3) &= \bar{\tau}_\beta(q; E_3) \int_0^\infty dk k^2 K_1^\ell(k, q; E_3) \frac{h_\alpha^\ell(k; E_3)}{(k^2 - k_\alpha^2 - i\epsilon)}, \end{aligned} \quad (\text{A14})$$

here  $q' = k_\beta = \sqrt{2\mu_{\beta(\alpha\alpha)}(E_3 - E_{\alpha\alpha})}$ , where  $h_\alpha$  represents the rearrangement and  $h_\beta$  represents the elastic scattering amplitudes.

## Appendix B: Scattering equation kernels

When using zero-range interactions, a momentum cut-off is required to regularize the integral equations for the  $s$ -wave state, within a renormalization procedure, where the binding energy of the triatomic molecule is kept fixed. For that, in the kernels a subtraction is performed with a regularizing momentum parameter  $\mu$  (see e.g. [95]), such that the kernels  $K_{1,2}$ ,  $\bar{\tau}_j$  and  $f_{\alpha,\beta}$  used in the bound-state and scattering equations are given by

$$\begin{aligned} K_{i=1,2}^\ell(q, k; E_3) &\equiv G_i^\ell(q, k; E_3) - G_i^\ell(q, k, -\mu^2) \delta_{i0}, \\ G_1^\ell(q, k; E_3) &= \int_{-1}^1 dx \frac{P_\ell(x)}{E_3 + i\epsilon - \frac{q^2}{m} - \frac{k^2}{2\mu_{\alpha\beta}} - \frac{kqx}{m}}, \\ G_2^\ell(q, k; E_3) &= \int_{-1}^1 dx \frac{P_\ell(x)}{E_3 + i\epsilon - \frac{q^2 + k^2}{2\mu_{\alpha\beta}} - \frac{kqx}{Am}}, \end{aligned} \quad (\text{B1})$$

$$\bar{\tau}_\alpha(q; E_3) \equiv \frac{\mu_{\alpha(\alpha\beta)}}{2\pi\mu_{\alpha\beta}^2} [\kappa_{\alpha\beta} + \kappa_{3,\alpha\beta}(E_3)], \quad (\text{B2})$$

$$\bar{\tau}_\beta(q; E_3) \equiv \frac{\mu_{\beta(\alpha\alpha)}}{2\pi\mu_{\alpha\alpha}^2} [\kappa_{\alpha\alpha} + \kappa_{3,\alpha\alpha}(E_3)], \quad (\text{B3})$$

where

$$\begin{aligned} \kappa_{\alpha\alpha} &\equiv \sqrt{-2\mu_{\alpha\alpha}E_{\alpha\alpha}}, \quad \kappa_{\alpha\beta} \equiv \sqrt{-2\mu_{\alpha\beta}E_{\alpha\beta}} \\ \kappa_{3\alpha\alpha}(E_3) &\equiv \sqrt{-2\mu_{\alpha\alpha} \left[ E_3 - \frac{q^2}{2\mu_{\beta(\alpha\alpha)}} \right]}, \\ \kappa_{3\alpha\beta}(E_3) &\equiv \sqrt{-2\mu_{\alpha\beta} \left[ E_3 - \frac{q^2}{2\mu_{\alpha(\alpha\beta)}} \right]}. \end{aligned} \quad (\text{B4})$$

$$\begin{aligned} f_\alpha &= \mu_{\alpha\beta} / \sqrt{k_{\alpha\beta}} \\ f_\beta &= \mu_{\alpha\alpha} / \sqrt{k_{\alpha\alpha}} \end{aligned} \quad (\text{B5})$$

In the case of the Yamaguchi separable potential from Eq. (19),  $K_{1,2}$  and  $\bar{\tau}_j$  are given by the following:

$$\begin{aligned} K_1^\ell(q, k; E_3) &= \int_{-1}^1 dx \left[ q^2 + \frac{k^2}{4} + qkx + \gamma_{\alpha\alpha}^2 \right]^{-1} \\ &\times \left[ k^2 + \frac{q^2 A^2}{(A+1)^2} + \frac{2qkAx}{(A+1)} + \gamma_{\alpha\beta}^2 \right]^{-1} \\ &\times \left[ E_3 + i\epsilon - \frac{q^2}{m} - \frac{k^2}{2\mu_{\alpha\beta}} - \frac{qkx}{m} \right]^{-1} P_\ell(x), \end{aligned} \quad (\text{B6})$$

$$\begin{aligned} K_2^\ell(q, k; E_3) &= \int_{-1}^1 dx \left[ k^2 + \frac{q^2}{(A+1)^2} + \frac{2qkx}{(A+1)} + \gamma_{\alpha\beta}^2 \right]^{-1} \\ &\times \left[ q^2 + \frac{k^2}{(A+1)^2} + \frac{2qkx}{(A+1)} + \gamma_{\alpha\beta}^2 \right]^{-1} \\ &\times \left[ E_3 + i\epsilon - \frac{(q^2 + k^2)}{2\mu_{\alpha\beta}} - \frac{qkx}{Am} \right]^{-1} P_\ell(x), \end{aligned} \quad (\text{B7})$$

$$\begin{aligned} \bar{\tau}_\alpha(q; E_3) &\equiv \frac{\mu_{\alpha(\alpha\beta)}}{\pi\mu_{\alpha\beta}^2} \left[ \frac{\gamma_{\alpha\beta}(\gamma_{\alpha\beta} + \kappa_{\alpha\beta})^2}{2\gamma_{\alpha\beta} + \kappa_{3\alpha\beta}(E_3) + \kappa_{\alpha\beta}} \right. \\ &\times \left. [\gamma_{\alpha\beta} + \kappa_{3\alpha\beta}(E_3)]^2 [\kappa_{\alpha\beta} + \kappa_{3\alpha\beta}(E_3)] \right], \end{aligned} \quad (\text{B8})$$

$$\begin{aligned} \bar{\tau}_\beta(q; E_3) &\equiv \frac{\mu_{\beta(\alpha\alpha)}}{\pi\mu_{\alpha\alpha}^2} \left[ \frac{\gamma_{\alpha\alpha}(\gamma_{\alpha\alpha} + \kappa_{\alpha\alpha})^2}{2\gamma_{\alpha\alpha} + \kappa_{3\alpha\alpha}(E_3) + \kappa_{\alpha\alpha}} \right. \\ &\times \left. [\gamma_{\alpha\alpha} + \kappa_{3\alpha\alpha}(E_3)]^2 [\kappa_{\alpha\alpha} + \kappa_{3\alpha\alpha}(E_3)] \right]. \end{aligned} \quad (\text{B9})$$

$$\begin{aligned} f_\alpha &= 2\pi\mu_{\alpha\beta} / \sqrt{k_{\alpha\beta}\gamma_{\alpha\beta}(k_{\alpha\beta} + \gamma_{\alpha\beta})^3} \\ f_\beta &= 2\pi\mu_{\alpha\alpha} / \sqrt{k_{\alpha\alpha}\gamma_{\alpha\alpha}(k_{\alpha\alpha} + \gamma_{\alpha\alpha})^3} \end{aligned} \quad (\text{B10})$$

In our approach, the parameters of the separable interactions are fixed by the corresponding bound-state energies, as well as by the effective ranges (when considering finite-range interactions).

## Appendix C: Cross-sections

The scattering observables are obtained from the scattering amplitudes, which for elastic reaction is  $U_{el} = U_{11} + U_{21}$  and for exchange reaction  $U_{ex} = \sqrt{2}U_{31}$ . For the elastic scattering, we write that:

$$\frac{d\sigma_{el}}{d\Omega} = (2\pi)^4 \mu_{\alpha(\alpha\beta)}^2 |\langle \mathbf{q}_f \phi_\alpha | U_{el} | \mathbf{q}_i \phi_\alpha \rangle|^2, \quad (\text{C1})$$

where  $\phi_\alpha$  is the bound state of  $\alpha\beta$  subsystem and  $q_i = q_f = \sqrt{-2\mu_{\alpha(\alpha\beta)}(E_3 - E_{\alpha\beta})} = \sqrt{-2\mu_{\alpha(\alpha\beta)}E_k}$ .

We will use the following relations between two-body bound state and the form factor when we are using the one-term separable potential:

$$V | \phi_\alpha \rangle = \lambda | g_\alpha \rangle \langle g_\alpha | \phi_\alpha \rangle = f_\alpha | g_\alpha \rangle; \quad (C2)$$

consequently, in subsystem  $\alpha\beta$  for on-shell momentum, we have:

$$\tau_{\alpha\beta}(k; E_3) = \frac{2\mu_{\alpha(\alpha\beta)}f_\alpha^2}{(k_\alpha^2 - k^2)}, \quad (k \rightarrow k_\alpha) \quad (C3)$$

and finally we can relate the transition amplitudes to our scattering function that we have calculate in Eq. (A10)

$$\begin{aligned} h_\alpha(\mathbf{k}; E_3) &= 2\pi^2 \bar{\tau}_{\alpha\beta}(k; E_3) X(\mathbf{k}, \mathbf{k}') \\ &= -4\pi^2 \mu_{\alpha(\alpha\beta)} f_\alpha^2 X(\mathbf{k}, \mathbf{k}') \\ &= -4\pi^2 \mu_{\alpha(\alpha\beta)} f_\alpha^2 \langle \mathbf{k} | \langle g_\alpha | G_0 U_{el} G_0 | g_\alpha \rangle | \mathbf{k}' \rangle \\ &= -4\pi^2 \mu_{\alpha(\alpha\beta)} f_\alpha^2 \langle \mathbf{k} \phi_\alpha | V G_0 U_{el} G_0 V | \mathbf{k}' \phi_\alpha \rangle / f_\alpha^2 \\ &= -4\pi^2 \mu_{\alpha(\alpha\beta)} \langle \mathbf{k} \phi_\alpha | U_{el} | \mathbf{k}' \phi_\alpha \rangle \end{aligned} \quad (C4)$$

considering all the above equations the elastic cross section can be written as follow:

$$\frac{d\sigma_{el}}{d\Omega} = |h_\alpha(\mathbf{k}; E_3)|^2, \quad (C5)$$

For the exchange reaction cross section we have:

$$\begin{aligned} \frac{d\sigma_{ex}}{d\Omega} &= (2\pi)^4 \mu_{\beta(\alpha\alpha)}^2 \sqrt{\frac{\mu_{\alpha(\alpha\beta)}}{\mu_{\beta(\alpha\alpha)}}} \sqrt{1 - \frac{E_{\alpha\alpha} - E_{\alpha\beta}}{E_k}} \\ &\times |\langle \mathbf{q}_f \phi_\beta | U_{ex} | \mathbf{q}_i \phi_\alpha \rangle|^2 \end{aligned} \quad (C6)$$

where  $q_f = \sqrt{2\mu_{\beta(\alpha\alpha)}(E_{\alpha\beta} - E_{\alpha\alpha} + E_k)}$ , with the same method we can show that

$$h_\beta(\mathbf{k}, E_3) = \frac{-8\pi^2 \mu_{\beta(\alpha\alpha)} f_\beta}{\sqrt{2} f_\alpha} \langle \mathbf{q}_f \phi_\beta | U_{ex} | \mathbf{q}_i \phi_\alpha \rangle, \quad (C7)$$

resulting in:

$$\frac{d\sigma_{ex}}{d\Omega} = \frac{f_\alpha^2}{2f_\beta^2} \sqrt{\frac{\mu_{\alpha(\alpha\beta)}}{\mu_{\beta(\alpha\alpha)}}} \sqrt{1 - \frac{E_{\alpha\alpha} - E_{\alpha\beta}}{E_k}} |h_\beta(\mathbf{k}; E_3)|^2. \quad (C8)$$

In the case of scattering of  $\beta$  from  $\alpha\alpha$  we need scattering amplitudes for elastic,  $U_{el} = U_{11}$ , and exchange channels,  $U_{ex} = (U_{21} + U_{31})$ , and the cross-sections are written as:

$$\frac{d\sigma_{el}}{d\Omega} = \frac{1}{4} |h_\beta(\mathbf{k}; E_3)|^2, \quad (C9)$$

and

$$\frac{d\sigma_{ex}}{d\Omega} = \frac{f_\beta^2}{2f_\alpha^2} \sqrt{\frac{\mu_{\beta(\alpha\alpha)}}{\mu_{\alpha(\alpha\beta)}}} \sqrt{1 - \frac{E_{\alpha\beta} - E_{\alpha\alpha}}{E_k}} |h_\alpha(\mathbf{k}; E_3)|^2, \quad (C10)$$

where  $h_\alpha$  and  $h_\beta$  are calculated from (A14).

- 
- [1] H. Feshbach(1958), Unified theory of nuclear reactions, *Annals of Physics* **5**, 357 (1958).
  - [2] S. Inouye, M. R. Andrews, J. Stenger, H.-J. Miesner, D.M. Stamper-Kurn, W. Ketterle, Observation of Feshbach resonances in a Bose-Einstein condensate, *Nature* **392**, 151 (1998).
  - [3] E. Timmermans, P. Tommasini, M. Hussein, and A. Kerman, Feshbach resonances in atomic Bose-Einstein condensates, *Phys. Rep.* **315**, 199 (1999).
  - [4] C. Chin, R. Grimm, P. Julienne, and E. Tiesinga, Feshbach resonances in ultracold gases, *Rev. Mod. Phys.* **82**, 1225 (2010).
  - [5] P. D. Lett, P. S. Julienne, and W. D. Phillips, Photoassociative spectroscopy of laser cooled atoms, *Ann. Rev. Phys. Chem.* **46**, 423 (1995).
  - [6] D. J. Heinzen, "Collisions of ultracold atoms in optical fields", in *Atomic Physics 14* (D. J. Wineland, C. E. Wieman, and S. J. Smith, Eds.), 369-388, AIP Press, New York, 1995.
  - [7] J. Weiner, V. S. Bagnato, S. C. Zilio, and P. S. Julienne, Experiments and theory in cold and ultracold collisions, *Rev. Mod. Phys.* **71**, 1 (1999).
  - [8] W. C. Stwalley and H. Wang, Photoassociation of ultracold atoms: A new spectroscopic technique, *Journal of Molecular Spectroscopy* **195**, 194 (1999).
  - [9] W. C. Stwalley, Collisions and reactions of ultracold molecules, *Can. J. Chem.* **82**, 709 (2004).
  - [10] S. Jochim, M. Bartenstein, A. Altmeyer, G. Hendl, S. Reidl, C. Chin, J. Hecker Denschlag, and R. Grimm, Bose-Einstein condensation of molecules, *Science* **302**, 2101 (2003).
  - [11] M. Greiner, C.A. Regal, and D.S. Jin, Emergence of a molecular Bose-Einstein condensate from a Fermi gas, *Nature* **426**, 537 (2003).
  - [12] T. Mukaiyama, J. R. Abo-Shaeer, K. Xu, J. K. Chin, and W. Ketterle, Dissociation and decay of ultracold sodium molecules, *Phys. Rev. Lett.* **92**, 180402 (2004).
  - [13] M. Guo, B. Zhu, B. Lu, X. Ye, F. Wang, R. Vexiau, N. Bouloufa-Maafa, G. Quémener, O. Dulieu, and D. Wang, Creation of an ultracold gas of ground-state dipolar  $^{23}\text{Na}^{87}\text{Rb}$  molecules, *Phys. Rev. Lett.* **116**, 205303 (2016).
  - [14] K. K. Voges, P. Gersema, T. Hartmann, T. A. Schulze, A. Zenesini and S. Ospelkaus, A pathway to ultracold bosonic  $^{23}\text{Na}^{39}\text{K}$  ground state molecules, *Phys. Rev. Lett.* **125**, 083401 (2020).
  - [15] A. Green, H. Li, J. H. S. Toh, X. Tang, K. C. McCormick, M. Li, E. Tiesinga, S. Kotochigova, and S. Gupta, Feshbach resonances in  $p$ -wave three-body recombination within Fermi-Fermi mixtures of open-shell  $^6\text{Li}$  and closed-shell  $^{173}\text{Yb}$  Atoms. *Phys. Rev. X* **10**, 031037 (2020).

- [16] P. Staunum, S. D. Kraft, J. Lange, R. Wester, and M. Weidemüller, Experimental investigation of ultracold atom-molecule collisions, *Phys. Rev. Lett.* **96**, 023201 (2006).
- [17] N. Zahzam, T. Vogt, M. Mudrich, D. Comparat, and P. A. Pillet, Atom-molecule collisions in an optically trapped gas, *Phys. Rev. Lett.* **96**, 023202 (2006).
- [18] F. Ferlaino, S. Knoop, M. Mark, M. Berninger, H. Schöbel, H.-C. Nägerl, and R. Grimm, Collisions between tunable halo dimers: exploring an elementary four-body process with identical bosons, *Phys. Rev. Lett.* **101**, 023201 (2008).
- [19] Y. Inada, M. Horikoshi, S. Nakajima, M. Kuwata-Gonokami, M. Ueda, and T. Mukaiyama, Collisional properties of  $p$ -wave Feshbach molecules *Phys. Rev. Lett.* **101**, 100401.
- [20] E. R. Hudson, N. B. Gilfoy, S. Kotochigova, J. M. Sage, and D. DeMille, Inelastic collisions of ultracold heteronuclear molecules in an optical trap, *Phys. Rev. Lett.* **100**, 203201 (2008).
- [21] R. V. Krems, Cold controlled chemistry, *Phys. Chem. Chem. Phys.* **10**, 4079 (2008).
- [22] L.D. Carr, D. DeMille, R.V. Krems, and J. Ye, Cold and ultracold molecules: science, technology and applications, *New J. Phys.* **11**, 055049 (2009).
- [23] S. Ospelkaus, K.-K. Ni, D. Wang, M. H. G. de Miranda, B. Neyenhuis, G. Quémener, P. S. Julienne, J. L. Bohn, D. S. Jin, and J. Ye, Quantum-state controlled chemical reactions of ultracold potassium-rubidium molecules, *Science* **327**, 853 (2010).
- [24] C. Klempt, T. Henninger, O. Topic, M. Scherer, L. Kattner, E. Tiemann, W. Ertmer, and J. J. Arlt, Radio-frequency association of heteronuclear Feshbach molecules. *Phys. Rev. A* **78**, 061602 (2008).
- [25] M. T. Bell and T. P. Softley, Ultracold molecules and ultracold chemistry. *Mol. Phys.* **107**, 99 (2009).
- [26] K.-K. Ni, S. Ospelkaus, D. Wang, G. Quémener, B. Neyenhuis, M. H. G. de Miranda, J. L. Bohn, J. Ye, and D. S. Jin, Dipolar collisions of polar molecules in the quantum regime, *Nature* **464**, 1324 (2010).
- [27] S. Knoop, F. Ferlaino, M. Berninger, M. Mark, H.-C. Nägerl, R. Grimm, J. P. D'Incao, and B. D. Esry, Magnetically controlled exchange process in an ultracold atom-dimer mixture. *Phys. Rev. Lett.* **104**, 053201 (2010).
- [28] T. Lompe, T. B. Ottenstein, F. Serwane, K. Viering, A. N. Wenz, G. Zürn, and S. Jochim, Atom-dimer scattering in a three-component Fermi gas. *Phys. Rev. Lett.* **105**, 103201 (2010).
- [29] S. Nakajima, M. Horikoshi, T. Mukaiyama, P. Naidon, and M. Ueda, Nonuniversal Efimov atom-dimer resonances in a three-component mixture of  $^6\text{Li}$ . *Phys. Rev. Lett.* **105**, 023201 (2010).
- [30] M. H. G. de Miranda, A. Chotia, B. Neyenhuis, D. Wang, G. Quémener, S. Ospelkaus, J. L. Bohn, J. Ye, and D. S. Jin, Controlling the quantum stereo-dynamics of ultracold bimolecular reactions. *Nat. Phys.* **7**, 502-507 (2011).
- [31] G. Quémener and P. S. Julienne, Ultracold molecules under control! *Chem. Rev.* **112**, 4949 (2012).
- [32] C.-H. Wu, J. W. Park, P. Ahmadi, S. Will, and M. W. Zwierlein, Ultracold fermionic Feshbach molecules of  $^{23}\text{Na}^{40}\text{K}$ , *Phys. Rev. Lett.* **109**, 085301 (2012).
- [33] T. T. Wang, M.-S. Heo, T. M. Rvachov, D. A. Cotta, and W. Ketterle, Deviation from universality in collisions of ultracold  $^6\text{Li}_2$  molecules, *Phys. Rev. Lett.* **110**, 173203 (2013).
- [34] J. Rui, H. Yang, L. Liu, D.-C. Zhang, Y.-X. Liu, J. Nan, Y.-A. Chen, B. Zhao, and J.-W. Pan, Controlled state-to-state atom-exchange reaction in an ultracold atom-dimer mixture, *Nature Physics* **13**, 699 (2017).
- [35] D. K. Hoffmann, T. Paintner, W. Limmer, D. S. Petrov, and J. H. Denschlag, Reaction kinetics of ultracold molecule-molecule collisions, *Nature Comm.* **9**, 5244 (2018).
- [36] C. Gao and P. Zhang, Atom-dimer scattering in a heteronuclear mixture with a finite intraspecies scattering length, *Phys. Rev. A* **97**, 042701 (2018).
- [37] H. Yang, D.-C. Zhang, L. Liu, Y.-X. Liu, J. Nan, B. Zhao, J.-W. Pan, Observation of magnetically tunable Feshbach resonances in ultracold  $^{23}\text{Na}^{40}\text{K}+^{40}\text{K}$  collisions, *Science* **363**, 261 (2019).
- [38] H. Li, M. Li, C. Makrides, A. Petrov, and S. Kotochigova, Universal Scattering of Ultracold Atoms and Molecules in Optical Potentials, *Atoms* **7**, 36 (2019).
- [39] B.-B. Wang, S.-H. Jing, and T.-X. Zeng, Cold atom-atom-anion three-body recombination of  $^4\text{He}^4\text{He}^x\text{Li}$  ( $x = 6$  or  $7$ ) systems, *J. Chem. Phys.* **150**, 094301 (2019).
- [40] L. A. Reynolds, E. Schwartz, U. Ebling, M. Weyland, J. Brand, and M. F. Andersen, Direct measurements of collisional dynamics in cold atom triads, *Phys. Rev. Lett.* **124**, 073401 (2020).
- [41] C. Makrides, D. S. Barker, J. A. Fedchak, J. Scherschligt, S. Eckel, and E. Tiesinga, Collisions of room-temperature helium with ultracold lithium and the van der Waals bound state of  $\text{HeLi}$ , *Phys. Rev. A* **101**, 012702 (2020).
- [42] V. Efimov, Energy levels arising from resonant two-body forces in a three-body system, *Phys. Lett.* **33 B**, 563 (1970).
- [43] M.A. Shalchi, A. Delfino, T. Frederico, and L. Tomio, Scattering of cold  $^4\text{He}$  on  $^4\text{He}$ ,  $^6,^7\text{Li}$  and  $^4\text{He}^{23}\text{Na}$  molecules, *Phys. Rev. A* **98**, 032705 (2018).
- [44] T.K. Lim, K. Duffy, and W.C. Damert, Efimov state in the  $^4\text{He}$  trimer, *Phys. Rev. Lett.* **38**, 341 (1977).
- [45] H.S. Huber and T.K. Lim, A study of the Efimov states and binding energies of the helium trimer through the Faddeev-coordinate-momentum approach, *J. Chem. Phys.* **68**, 1006 (1978).
- [46] H.S. Huber, T.K. Lim, and D.H. Feng, Search for Efimov states in  $^{12}\text{C}$ , *Phys. Rev. C* **18**, 1534(R) (1978).
- [47] S. Nakaichi-Maeda and T.K. Lim, Zero-energy scattering and bound states in the  $^4\text{He}$  trimer and tetramer, *Phys. Rev. A* **28**, 692 (1983).
- [48] Th. Cornelius and W. Glöckle, Efimov states for three  $^4\text{He}$  atoms? *J. Chem. Phys.* **85**, 3906 (1986).
- [49] J. Yuan and C.D. Lin, Weakly bound triatomic  $\text{He}_2\text{Li}$  and  $\text{He}_2\text{Na}$  molecules, *J. Phys. B: At. Mol. Opt. Phys.* **31**, L637 (1998).
- [50] T. Frederico, L. Tomio, A. Delfino, and A.E.A. Amorim, Scaling limit of weakly bound triatomic states, *Phys. Rev. A* **60**, R9 (1999).
- [51] P. Stipanović, L. Vranješ Markić, I. Bešlić, I. and J. Boronat, Universality in Molecular Halo Clusters, *Phys. Rev. Lett.* **113**, 253401 (2014).
- [52] P. Stipanović, L. Vranješ Markić, A. Gudyma and J. Boronat, Universality of size-energy ratio in four-body

- systems, *Scientific Reports* **9**, 6289 (2019).
- [53] S. Huber, Efimov states in  $^4\text{He}$  trimers by two-body effective-range and scattering-length analysis: A comparison with Faddeev calculations, *Phys. Rev. A* **31**, 3981 (1985).
  - [54] B.D. Esry, C.D. Lin, C.H. Greene, Adiabatic hyperspherical study of the helium trimer, *Phys. Rev. A* **54**, 394 (1996).
  - [55] E.A. Kolganova, A.K. Motovilov, and S.A. Sofianos, Ultralow energy scattering of a He atom off a He dimer, *Phys. Rev. A* **56**, R1686 (1997).
  - [56] A.K. Motovilov, W. Sandhas, S.A. Sofianos, E.A. Kolganova, Binding energies and scattering observables in the  $^4\text{He}_3$  atomic system, *Eur. Phys. J. D* **13**, 33 (2001).
  - [57] E.A. Kolganova, A.K. Motovilov, W. Sandhas, Scattering length of the helium-atom–helium-dimer collision, *Phys. Rev. A* **70**, 052711 (2004).
  - [58] A. Delfino, T. Frederico, and L. Tomio, Prediction of a weakly bound excited state in the  $^4\text{He}$ – $^7\text{Li}$  molecule, *J. Chem. Phys.* **113**, 7874 (2000).
  - [59] I. Baccarelli, G. Delgado-Barrio, F. A. Gianturco, T. González-Lezana, S. Miret-Artés, and P. Villarreal, Searching for Efimov states in triatomic systems: The case of  $\text{LiHe}_2$ , *Europhys. Lett.* **50**, 567 (2000).
  - [60] C. Di Paola, F. A. Gianturco, F. Paesani, G. Delgado-Barrio, S. Miret-Artés, P. Villarreal, I. Baccarelli, and T. González-Lezana, Ground states of weakly bound three-atom systems: energies and shapes of  $^4\text{He}_2\text{X}$  clusters from Monte Carlo calculations, *J. Phys. B: At. Mol. Opt. Phys.* **35**, 2643 (2002).
  - [61] V. Roudnev and M. Cavagnero, Benchmark helium dimer and trimer calculations with a public few-body code, *J. Phys. B: At. Mol. Opt. Phys.* **45**, 025101 (2012).
  - [62] M.-S. Wu, H.-L. Han, C.-B. Li, and T.-Y. Shi, Prediction of a weakly bound excited state of Efimov character in a  $^7\text{Li}^4\text{He}_2$  system, *Phys. Rev. A* **90**, 062506 (2014).
  - [63] E. A. Kolganova, A. K. Motovilov, and W. Sandhas, The  $4\text{He}$  trimer as an Efimov system: Latest developments, *Few-Body Syst.* **58**, 35 (2017).
  - [64] E. A. Kolganova, Faddeev calculation of helium atom– $\text{LiHe}$ -dimer scattering Length, *Few-Body Syst* (2018) **59**, 28 (2018).
  - [65] F. Luo, G. Kim, G. C. McBane, C. F. Giese, and W. R. Gentry, Influence of retardation on the vibrational wave function and binding energy of the helium dimer, *J. Chem. Phys.* **98**, 9687 (1993).
  - [66] W. Schöllkopf and J. P. Toennies, Nondestructive mass selection of small van der Waals clusters, *Science* **266**, 1345 (1994).
  - [67] R. E. Grisenti, W. Schöllkopf, J.P. Toennies, G.C. Hegerfeldt, T. Köhler, M. Stoll, Determination of the bond length and binding energy of the helium dimer by diffraction from a transmission grating, *Phys. Rev. Lett.* **85**, 2284 (2000).
  - [68] M. Kunitski *et al.*, Observation of the Efimov state of the helium trimer, *Science* **348**, 551 (2015).
  - [69] M. Zaccanti, B. Deissler, C. D’Errico, M. Fattori, M. Jona-Lasinio, S. Müller, G. Roati, M. Inguscio, and G. Modugno, Observation of an Efimov spectrum in an atomic system, *Nat. Phys.* **5**, 586 (2009).
  - [70] S.E. Pollack, D. Dries and R.G. Hulet, Universality in three- and four-body bound states of ultracold atoms, *Science* **326**, 1683 (2009).
  - [71] S. Knoop, F. Ferlaino, M. Mark, M. Berninger, H. Schöbel, H.-C. Nägerl, and R. Grimm, Observation of an Efimov-like trimer resonance in ultracold atom-dimer scattering, *Nat. Phys.* **5**, 227 (2009).
  - [72] G. Barontini, C. Weber, F. Rabatti, J. Catani, G. Thalhammer, M. Inguscio, and F. Minardi, Observation of heteronuclear atomic Efimov resonances, *Phys. Rev. Lett.* **103**, 043201 (2009); Erratum: *Phys. Rev. Lett.* **104**, 059901(E) (2010).
  - [73] R.S. Bloom, M.-G. Hu, T.D. Cumby, D.S. Jin, Tests of universal three-body physics in an ultracold Bose-Fermi mixture, *Phys. Rev. Lett.* **111**, 105301 (2013).
  - [74] R. Pires, J. Ulmanis, S. Häfner, M. Repp, A. Arias, E.D. Kuhnle, M. Weidemüller, Observation of Efimov resonances in a mixture with extreme mass imbalance, *Phys. Rev. Lett.* **112**, 250404 (2014).
  - [75] J. Ulmanis, S. Häfner, E.D. Kuhnle, M. Weidemüller, Heteronuclear Efimov resonances in ultracold quantum gases, *Natl. Sci. Rev.* **3**, 174 (2016).
  - [76] F. Bringas, M.T. Yamashita, T. Frederico, Triatomic continuum resonances for large negative scattering lengths, *Phys. Rev. A* **69**, 040702 (2004).
  - [77] Y. Wang, J. P. D’Incao, H.-C. Nägerl, and B. D. Esry, Colliding Bose-Einstein condensates to observe Efimov physics, *Phys. Rev. Lett.* **104**, 113201 (2010).
  - [78] J. Levinsen and D.S. Petrov, Atom-dimer and dimer-dimer scattering in fermionic mixtures near a narrow Feshbach resonance, *Eur. Phys. J. D* **65**, 67-82 (2011).
  - [79] E. Garrido, C. Romero-Redondo, A. Kievsky, M. Viviani, Integral relations and the adiabatic expansion method for 1+2 reactions above the breakup threshold: Helium trimers with soft-core potentials *Phys. Rev. A* **86**, 052709 (2012).
  - [80] D. Blume and Y. Yan, Generalized Efimov scenario for heavy-light mixtures, *Phys. Rev. Lett.* **113**, 213201 (2014).
  - [81] M.A. Shalchi, M.T. Yamashita, M.R. Hadizadeh, E. Garrido, L. Tomio, and T. Frederico, Probing Efimov discrete scaling in an atom-molecule collision, *Phys. Rev. A* **97**, 012701 (2018).
  - [82] A. Gammal, T. Frederico, L. Tomio, and Ph. Chomaz, Liquid-gas phase transition in Bose-Einstein condensates with time evolution, *Phys. Rev. A* **61**, 051602(R) (2000);
  - [83] L. D. Faddeev, *Mathematical aspects of the three body problem in Quantum Scattering Theory*, Davey, New York, 1965.
  - [84] A.E.A. Amorim, T. Frederico, and L. Tomio, Universal aspects of Efimov states and light halo nuclei, *Phys. Rev. C* **56**, R2378 (1997).
  - [85] Y. Yamaguchi, Two-nucleon problem when the potential is nonlocal but separable. I *Phys. Rev.* **95**, 1628 (1954).
  - [86] H. Suno, Structure of the weakly bound triatomic  $\text{He}_2\text{Li}$  and  $\text{He}_2\text{Na}$  molecules, *Phys. Rev. A* **96**, 012508 (2017).
  - [87] E. O. Alt, P. Grassberger and W. Sandhas, Reduction of the three-particle collision problem to multi-channel two-particle Lippmann-Schwinger equations, *Nucl. Phys. B* **2**, 167 (1967).
  - [88] W. Glöckle, *The Quantum Mechanical Few-Body Problem*. Springer-Verlag Berlin Heidelberg, New York Tokyo, 1983.
  - [89] U. Kleinekathöfer, M. Lewerenz, and M. Mladenović, Long range binding in alkali-helium pairs, *Phys. Rev. Lett.* **83**, 4717 (1999).

- [90] U. Kleinekathöfer, K. Tang, J. Toennies, and C. Yiu, Potentials for some rare gas and alkali-helium systems calculated from the surface integral method, *Chem. Phys. Lett.* **249**, 257 (1996).
- [91] U. Kleinekathöfer, K. T. Tang, J. P. Toennies, and C. L. Yiu, Van der Waals potentials of  $\text{He}_2$ ,  $\text{Ne}_2$ , and  $\text{Ar}_2$  with the exchange energy calculated by the surface integral method, *J. Chem. Phys.* **107**, 9502 (1997).
- [92] K. T. Tang, J. P. Toennies, and C. L. Yiu, Accurate analytical He-He van der Waals potential based on perturbation theory, *Phys. Rev. Lett.* **74**, 1546 (1995).
- [93] R. A. Aziz and M. J. Slaman, An examination of ab initio results for the helium potential energy curve, *J. Chem. Phys.* **94**, 8047 (1991).
- [94] D. Cvetko, A. Lausi, A. Morgante, F. Tommasini, P. Cortona, and M. G. Dondi, A new model for atom-atom potentials, *J. Chem. Phys.* **100**, 2052 (1994).
- [95] T. Frederico, A. Delfino, L. Tomio, M.T. Yamashita, Universal aspects of light halo nuclei, *Prog. Part. Nucl. Phys.* **67**, 939 (2012).
- [96] W. de Paula, T. Frederico, A. Delfino and L. Tomio, Limit cycles in the spectra of mass imbalanced many-boson system, *J. Phys. B: At. Mol. Opt. Phys.* **45**, 025101 (2020).
- [97] D. S. Rosa, T. Frederico, G. Krein, M. T. Yamashita, Efimov effect in D spatial dimensions in systems, *Phys. Rev. A* **97**, 050701 (2018).
- [98] A. Mohapatra and E. Braaten, Conformality lost in Efimov physics, *Phys. Rev. A* **98**, 013633 (2018).
- [99] E. Garrido, A. S. Jensen, R. Álvarez-Rodríguez, Few-body quantum method in a d-dimensional space *Phys. Lett. A* **383**, 2021 (2019).
- [100] S. R. Beane and M. Jafry, Dimensional crossover in non-relativistic effective field theory, *J. Phys. B: At. Mol. Opt. Phys.* **52**, 035001 (2019).